日本DDS学会理事長の橋田　充先生，第25回日本DDS学会学術集会会長の松村保広先生をはじめとする関係の諸先生方に心より御礼を申し上げます．

文　献

1) Hanash S : Disease proteomics. Nature 422 : 226-232, 2003.
2) Aderka D, Engelmann H, Maor Y, Brakebusch C, Wallach D : Stabilization of the bioactivity of tumor necrosis factor by its soluble receptors. J Exp Med 175 : 323-329, 1992.
3) Feldmann M, Maini R N : Lasker Clinical Medical Research Award. TNF defined as a therapeutic target for rheumatoid arthritis and other autoimmune diseases. Nat Med 9 : 1245-1250, 2003.
4) Muto Y, Nouri-Aria K T, Meager A, Alexander G J, Eddleston A L et al. : Enhanced tumour necrosis factor and interleukin-1 in fulminant hepatic failure. Lancet 2 : 72-74, 1988.
5) Breedveld F C, Emery P, Keystone E, Patel K, Furst D E et al. : Infliximab in active early rheumatoid arthritis. Ann Rheum Dis 63 : 149-155, 2004.
6) Genovese M C, Bathon J M, Martin R W, Fleischmann R M, Tesser J R et al. : Etanercept versus methotrexate in patients with early rheumatoid arthritis : two-year radiographic and clinical outcomes. Arthritis Rheum 46 : 1443-1450, 2002.
7) Gomez-Reino J J, Carmona L, Valverde V R, Mola E M, Montero M D : Treatment of rheumatoid arthritis with tumor necrosis factor inhibitors may predispose to significant increase in tuberculosis risk : a multicenter active-surveillance report. Arthritis Rheum 48 : 2122-2127, 2003.
8) Lubel J S, Testro A G, Angus P W : Hepatitis B virus reactivation following immunosuppressive therapy : guidelines for prevention and management. Intern Med J 37 : 705-712, 2007.
9) Sicotte N L, Voskuhl R R : Onset of multiple sclerosis associated with anti-TNF therapy. Neurology 57 : 1885-1888, 2001.
10) Mori L, Iselin S, De Libero G, Lesslauer W : Attenuation of collagen-induced arthritis in 55-kDa TNF receptor type 1 (TNFR1)-IgG1-treated and TNFR1-deficient mice. J Immunol 157 : 3178-3182, 1996.
11) Kassiotis G, Kollias G : Uncoupling the proinflammatory from the immunosuppressive properties of tumor necrosis factor (TNF) at the p55 TNF receptor level : implications for pathogenesis and therapy of autoimmune demyelination. J Exp Med 193 : 427-434, 2001.
12) Liu J, Marino M W, Wong G, Grail D, Dunn A, et al. : TNF is a potent anti-inflammatory cytokine in autoimmune-mediated demyelination. Nat Med 4 : 78-83, 1998.

参考文献

本稿の内容は，下記の論文等に詳細を報告している．

- Kamada H, Tsutsumi Y, Sato-Kamada K, Yamamoto Y, Yoshioka Y et al. : Synthesis of a poly(vinylpyrrolidone-co- dimethyl maleic anhydride) co-polymer and its application as renal targeting carrier. Nat Biotechnol 21 : 399-404, 2003.
- Yamamoto Y, Tsutsumi Y, Yoshioka Y, Nishibata T, Kobayashi K et al. : Site-specific PEGylation of a lysine-deficient TNF-alpha with full bioactivity. Nat Biotechnol 21 : 546-552, 2003.
- Kaneda Y, Tsutsumi Y, Yoshioka Y, Kamada H, Yamamoto Y et al. : The use of PVP as a polymeric carrier to improve the plasma half-life of drugs. Biomaterials 25 (16) : 3259-3266, 2004.
- Kodaira H, Tsutsumi Y, Yoshioka Y, Kamada H, Kaneda Y et al. : The targetting of anionized polyvinylpyrrolidone to the renal system. Biomaterials 25 : 4309-4315, 2004.
- Kamada H, Tsutsumi Y, Yoshioka Y, Yamamoto Y, Kodaiara H et al. : Design of a pH-sensitive polymeric carrier for drug release and its application in cancer therapy. Clin Cancer Res 10(7) : 2545-2550, 2004.
- Shibata H, Yoshioka Y, Ikemizu S, Kobayashi K, Yamamoto Y et al. : Functionalization of TNF-alpha using phage display technique and PEGylation improves its antitumor therapeutic window. Clin Cancer Res 10 (24) : 8293-8300, 2004.
- Shibata H, Yoshioka Y, Ohkawa A, Minowa K, Mukai Y et al. : Creation and X-ray structure analysis of the tumor necrosis factor receptor-1-selective mutant of a tumor necrosis factor-alpha antagonist. J Biol Chem 283 : 998-1007, 2008.
- Yoshikawa T, Sugita T, Mukai Y, Yamanada N, Nagano K et al. : Organelle-targeted delivery of biological macromolecules using the protein transduction domain : Potential applications for peptide aptamer delivery into the nucleus. J Mol Biol 380(5) : 777-782, 2008.
- Mukai Y, Shibata H, Nakamura T, Yoshioka Y, Abe Y et al. : Structure-function relationship of tumor necrosis factor (TNF) and its receptor interaction based on 3D structural analysis of a fully active TNFR1-selective TNF mutant. J Mol Biol, in press.
- Yoshikawa T, Sugita T, Mukai Y, Yamanada N, Nagano K et al. : The augmentation of intracellular delivery of peptide therapeutics by artificial protein transduction domains. Biomaterials, in press.
- Kayamuro H, Yoshioka Y, Katayama K, Hiroi T, Nomura T et al. : Mutant TNF-a as mucosal vaccine adjuvants enhance antigen specific IgA immune responses in mice. Biomaterials, in press.

第2章 先端科学技術とDDS開発

3 プロテオーム解析とタンパク質DDSの設計・評価

Drug delivery systems for proteomics-based drug innovation

独立行政法人医薬基盤研究所[1]，大阪大学大学院薬学研究科[2]
長野一也[1]，阿部康弘[1]，角田慎一[1,2]，堤　康央[1,2]
KAZUYA NAGANO[1], YASUHIRO ABE[1], SHIN-ICHI TSUNODA[1,2], YASUO TSUTSUMI[1,2]
National Institute of Biomedical Innovation[1], Graduate School of Pharmaceutical Sciences, Osaka University[2]

はじめに

2003年にヒトゲノム解読が完了したものの，一般に遺伝子は設計図に過ぎず，RNAとして機能する例外を除き，これら遺伝子の機能を具現するのは，最終産物である蛋白質である。蛋白質は，「翻訳調節や翻訳後修飾」を受けるため，mRNAと蛋白質の間には，量的な相関関係は成立しないことが多い。特に，蛋白質の酸化的修飾やリン酸化等に伴う“蛋白質の機能変化・異常”は，後天的な疾患の発症や悪化の主因となっている。そのため先天的な遺伝子疾患等を除き，病態メカニズム等を解明しようとする生命科学研究では，遺伝子（ゲノム・トランスクリプトーム）の解析研究だけでは不十分であり，蛋白質（プロテオーム）の解析研究への期待が高まっている[1]。

細胞や個体においては，約2万数千種類の遺伝子の翻訳産物が種々修飾を受け，結果として10万種類以上にも及ぶ蛋白質として存在し，このうち数千種類が機能的に発現しているものと推定されている。これら発現蛋白質の「種類」や「量」，「時空間的な局在性」を網羅的に解析することで，健常状態における挙動とは異なった蛋白質を探索し，細胞や個体の状態（分化・老化・病態）情報を理解しようとする研究が，プロテオーム解析（プロテオミクス）であり，生命現象や種々疾患の解明のみならず，得られた情報・知見を活用し，安全性と有効性に優れた医薬品の開発等に展開していくことが期待されている。

このようなプロテオミクス研究の中でも，①疾患の発症や悪化といった病態の推移や合併症の発症，医薬品の効果や副作用を予測・評価できる疾患バイオマーカーの探索，②疾患の発症や悪化に関与している創薬ターゲットあるいは疾患の治癒に関わる医薬品シーズとなる蛋白質の探索は，資源に乏しく，知的創発に頼らざるを得ないわが国にとって，国民の健康と福祉の向上のみならず，知的財産立国・技術立国を標榜していくためにも，生命線と位置づけられている。しかしながら，遺伝子解析研究で欧米に出遅れたわが国は，上記の創薬プロテオミクス研究においても立ち後れているのが現状である。

1．創薬プロテオミクス研究の現状

種々難病に対する“疾患バイオマーカー”や“創薬ターゲット／医薬品シーズ”の探索は，臨床現場で最適医療を提供するだけでなく，安全かつ有効な医薬品の開発に際しての圧倒的な競争力の獲得に直結するため，これまでに類を見ないほどに，熾烈な国際競争が繰り広げられている。中でも，欧米各国はすでに，2000年以降，大量の国家予算を投じ，メガファーマ等を巻き込んで，創薬プロテオミクス研究に大規模着手している。ゲノム創薬で出遅れたわが国にとってこれは深刻な状況であり，この劣勢を挽回し，国際競争力に満ち溢れた画期的な医薬品開発を支援することを目的に，2003年，厚生労働省および国立医薬品食品衛生研究所（2005年以降は，独立行政法人医薬基盤研究所）が中心となり，製薬メーカー

22社，5カ所の国立センター，大阪大学医学部／蛋白質研究所といった産官学が強固に連携し，国家プロジェクト『疾患関連蛋白質解析研究事業』が開始された。本研究事業は，わが国の主要疾患等に関して，㋐患者(薬物治療中の患者を含む)と健常人との間で，質的，量的，時空間的に発現変動している蛋白質を解析し，㋑数多くの発現変動蛋白質の中から，疾患バイオマーカーや創薬ターゲット／医薬品シーズとなり得る蛋白質を絞り込み，㋒これらをバリデーションしたうえで，㋓新規医薬品の創出等に有効活用しようとするものである。当事業は，2008年度より，第2期事業に移行し，㋔医薬品等の毒性発現に起因して発現変動する安全性バイオマーカーの同定と安全な医薬品の開発支援をも目指した『創薬バイオマーカー探索研究事業』として再スタートしている。

2．抗体プロテオミクス技術

しかし残念ながら，世界的に観ても創薬プロテオミクス研究に成功した例はいまだ数少ないのが現状である。これはまず，疾患の発症や悪化，医薬品の有効性／毒性発現の際には，細胞・個体内に存在している数千種類の蛋白質のうち，数百種類以上もの蛋白質が質的，量的，時空間的に発現変動し，この中から真に意味のある『創薬バイオマーカーや創薬ターゲット／医薬品シーズ』の候補となる蛋白質を絞り込まねばならないことに起因している。すなわち，候補蛋白質の絞り込みを実現していくためには，数多くの発現変動蛋白質の機能・局在解析と病態・薬効・毒性との連関追求が不可欠であり，ほとんどの場合，個々の発現変動蛋白質に対しておのおののモノクローナル抗体を作製して，バリデーションすることが必須となる。そのため，例えば千種類の発現変動蛋白質が探索されてきた場合，千種類のモノクローナル抗体を作製せねばならない。一般にモノクローナル抗体作製には，一種類の蛋白質に対してすら，マウス等への免疫やハイブリドーマの作製，スクリーニング等の段階が必要であり，多くの場合，半年以上も要してしまう。これが，創薬プロテオミクス研究の大きな足かせになってしまっている。この問題は，創薬を志向したオミクス研究全般に当てはまることである。

また上記の抗体作製に関する諸課題を克服し，『創薬バイオマーカーや創薬ターゲット／医薬品シーズ』の候補蛋白質が絞り込まれた後には，疾患情報(がんの組織浸潤や転移の有無，合併症の併発，予後等)や薬効情報(抗がん剤の有効性／耐性等)，有害事象の情報(毒性発現の有無等)と，候補蛋白質の発現分布との連関をバリデーションし，有用な『創薬バイオマーカーや創薬ターゲット／医薬品シーズ』を同定せねばならない。しかし，このバリデーションに関しても，膨大な数の臨床検体に

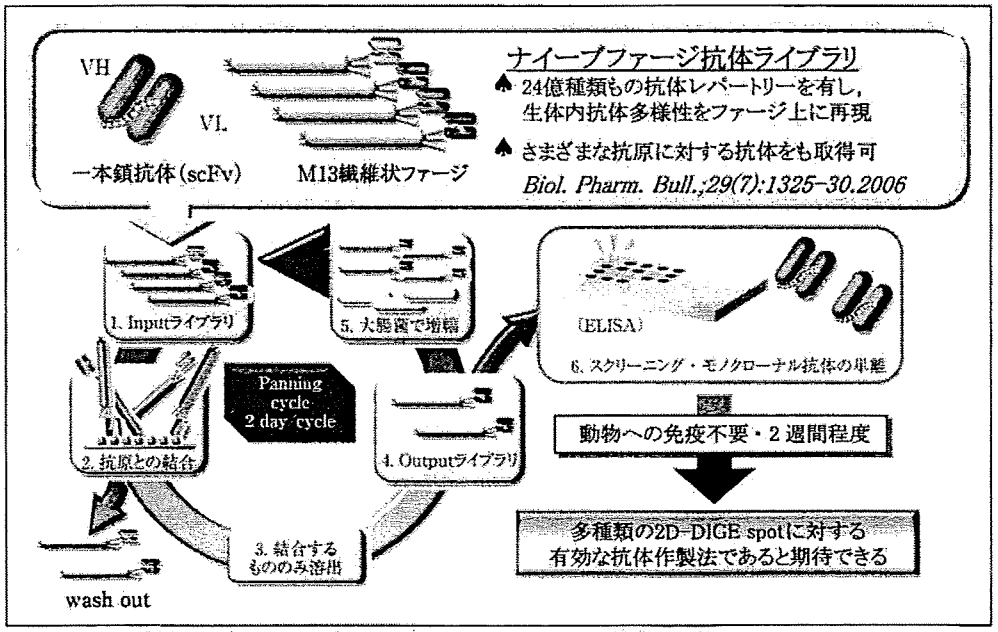

図1　ナイーブファージ抗体ライブラリの構築とモノクローナル抗体の単離
生体内抗体多様性をファージ上に再現し，理論上いかなる抗原に対しても抗体が単離可能なナイーブファージ抗体ライブラリを独自に作製した(24億種類のレパートリー)。抗体の単離にあたっては，ライブラリの中から抗原に結合するクローンを回収・濃縮し，その中からELISA等によって陽性クローンを選別する。

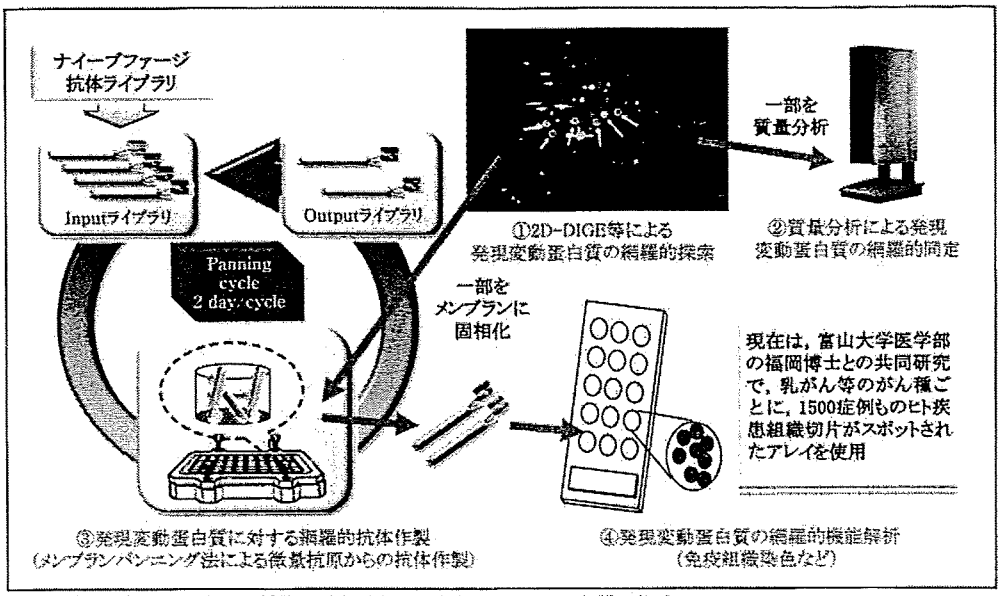

図2　抗体プロテオミクス技術による創薬バイオマーカー蛋白質の探索
ファージ抗体ライブラリによる*in vitro*抗体作製法をプロテオミクスに応用することで，これまで達成困難であった2D-DIGE spot中の微量で多数の発現変動蛋白質に対する網羅的な抗体作製を実現し，多数の発現変動蛋白質のハイスループットなバリデーションが可能となった。

頼らざるを得ないのが現状である。

この点，われわれは理論上生体内のあらゆる抗原に対する抗体を含んだ独自のファージ抗体ライブラリ(24億種類の抗体レパートリー)を開発するとともに，プロテオーム解析サンプルから直接回収される微量(0.5ng程度)かつ多種類の発現変動蛋白質から，おのおのの特異的モノクローナル抗体をわずか2週間程度で単離できる方法を考案した(図1)。得られたファージ抗体は，ELISAや免疫染色をはじめとする機能解析に展開可能である。われわれは現在，臨床情報既知(病態ステージ，予後，転移等)で，かつ1,500症例以上のヒト病態組織がスポットされた組織アレイ(富山大学医学部 福岡順也博士との共同研究)を用い，バリデーションを一挙に実施している。このヒト臨床検体の前処理から，プロテオーム解析による発現変動蛋白質の同定，抗体作製とバリデーションまでの過程を，約2～3週間で完了できるシステムを，われわれは“抗体プロテオミクス技術”と呼んでいる(図2)。この抗体プロテオミクス技術は，多数の発現変動蛋白質を質量分析器で同定すると同時に，その特異的モノクローナル抗体をおのおの作製し，臨床情報を豊富に搭載した“多数のヒト症例”に対し，一挙かつリアルタイムにバリデーションできる唯一の方法であり，先述した創薬プロテオミクス研究の諸問題を解決できる等，他を圧倒する競争力を有している。現在，乳がん・大腸がん・肺がん等を対象に，産官学の連携のもと，抗体プロテオミクス研究を推進しており，いくつかの興味深いバイオマーカー蛋白質を見出している。

3．ファージ表面提示法を利用した生物学的DDS

創薬プロテオミクス研究の成果を社会に還元していくためには，迅速かつ的確な病態診断により疾患予備軍の健康を保持するとともに，適切かつ安心できる治療計画の立案と治療モニタリングに有用な診断薬の開発が必須となる。この点，臨床情報と連関した創薬バイオマーカーは，国民の健康と医療現場にパラダイムシフトをもたらすであろう。また製薬メーカー等においては，新規産業シーズの獲得と，開発段階から高度に有効性と安全性が保証された画期的医薬品の開発を強力にサポートするものと期待される。一方で，医薬品シーズ／創薬ターゲットとなる蛋白質を有効活用した創薬に関しては，すでに数多くの事例が物語っているように，有効性と安全性を高度に保証していこうとする観点から，DDSの重要性がますます高まってくるものと考えられる。ここでは，われわれの種々DDS研究の中から(図3)，自己免疫疾患の発症・悪化における創薬ターゲット(腫瘍壊死因子：TNF)を一例に，創薬プロテオミクス研究の成果を有効活用しようとするDDSについて紹介する。

慢性関節リウマチや多発性硬化症等の自己免疫疾患は，

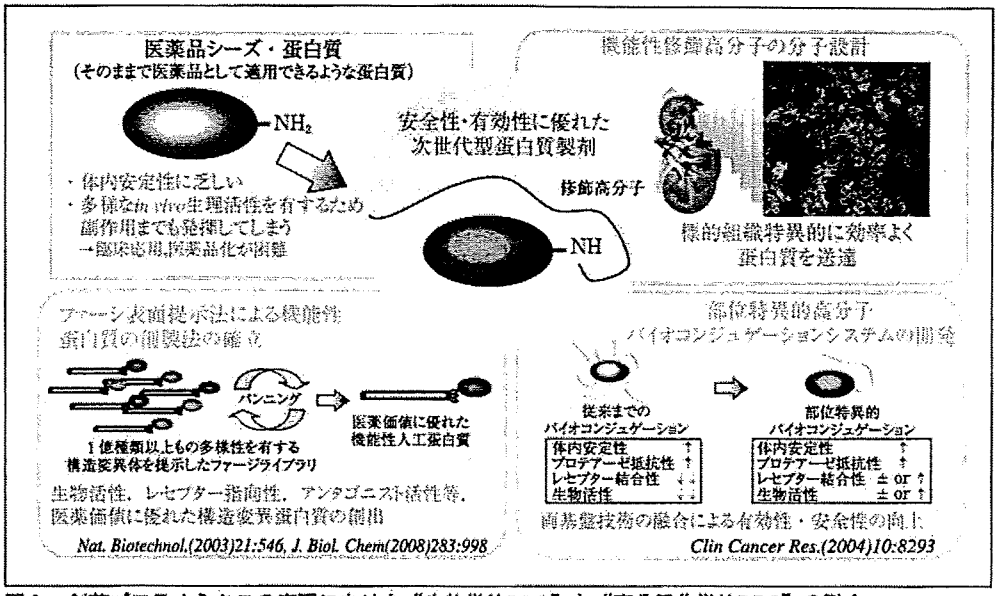

図3　創薬プロテオミクスの実現に向けた"生物学的DDS"と"高分子化学的DDS"の融合
ファージ表面提示法を駆使することにより，目的の受容体に選択的に結合可能な構造変異蛋白質の創出技術とリジン欠損構造変異蛋白質のN末端特異的な高分子バイオコンジュゲーションシステムの開発を実現し，これまで蛋白質の医薬品化において問題となっていた複数の受容体を介した多様な生理作用による副作用発現と体内安定性の乏しさによる大量頻回投与を一挙に克服することが可能になった。

いまだ克服すべき難病の1つとして広く認識されている。そのため，自己免疫疾患を標的とした創薬プロテオミクス研究が盛んに行われており，広範な炎症の惹起・悪化における主要な分子の1つとして，TNFが創薬ターゲットとなっている[2~4]。一方でTNFは，発がんや種々感染症に対する生体防御活性の中心を担っていることも明らかとなっているが，病態の発症・悪化と生体防御活性の発揮の調節メカニズムは，いまだ不明のままである。特にTNFの生体における2種類の存在形式(可溶型TNFと膜結合型TNF)の意義に加え，これらTNFに対する2種類のレセプター(TNFR1とTNFR2)を介した機能の相違等は十分に理解されていない。

現在，慢性関節リウマチに対する特効薬として，TNFに対する中和抗体や可溶型レセプターが，臨床に供されている。これら医薬品は，内因性TNFのすべての活性を遮断するものであり，リウマチ患者のQOLを格段に向上させる等，切れ味鋭い治療成績を発揮している[5,6]。しかしTNFは本来，宿主の生体防御機構に重要な役割を担っているため，これら抗TNF蛋白医薬の使用は，結核等の感染症や発がんに対する宿主の抵抗性を減弱させてしまい，臨床現場における大きな懸念事項となっている[7,8]。事実，因果関係等の科学的検証を今後必要とするものの，本邦において2007年12月に抗TNF蛋白医薬投与患者における死亡例が報告されている。また自己免疫疾患の中でも，多発性硬化症では，これら抗TNF蛋白医薬の使用は禁忌である[9]。

前述したように，TNFが結合するレセプターにはTNFR1とTNFR2が存在し，各レセプターが可溶型／膜結合型TNFと作用しつつ，非常に複雑かつ巧妙にその生体内反応が，正負に制御されている。われわれは現在，病態の発症や悪化に関わるTNF/TNFR結合のみを選択的に阻害できる抗TNF蛋白医薬の開発を目指して，可溶型／膜結合型TNFのTNFR1もしくはTNFR2を介した機能を解析し，宿主の生体防御機構や種々炎症反応の惹起・鎮静との連関追求を産官学と共同で実施しており，興味深い知見を集積しつつある。またこれまでの報告にもあるように，可溶型TNFのTNFR1を介した過剰な活性発現が炎症反応の惹起・悪化に，可溶型／膜結合型TNFのTNFR2を介した活性発現がウイルス感染防御や多発性硬化症の抑制に関与していることが明らかとなりつつある[10~12]。これは，可溶型TNFのTNFR1を介した活性発現を選択的に阻害することができれば，慢性関節リウマチのみならず，多発性硬化症等の自己免疫疾患にも有用かつ安全な医薬品が開発可能であることを示唆するものである。

この点，われわれはこれまでに，ファージ表面提示法を駆使することにより1億種類以上もの多様性を有した構造変異蛋白質ライブラリを一挙に構築し，この中から，

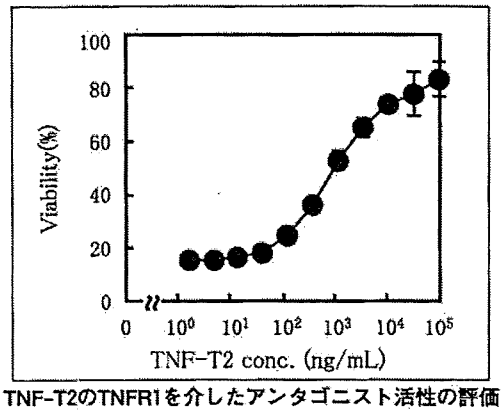

図4 TNF-T2のTNFR1を介したアンタゴニスト活性の評価 (L-M assay)

各濃度のTNF-T2をヒトwtTNF(5 ng/mL)と混ぜ，L-M細胞に添加した。
18時間後，wtTNFの細胞傷害性に対するTNF-T2の阻害効果をメチレンブルーアッセイにより評価した。wtTNF非添加群を100% Viabilityとした。

レセプター親和性(選択性／特異性)や体内安定性，生物活性を向上あるいは任意に制御した"機能性人工蛋白質"を迅速かつ効率良く創出できる「蛋白質分子進化システム」を確立している。本システムは，血中安定性の向上に加え，生物学的改変により特定のレセプターへのターゲティング能を蛋白質に付与できる点で，分子レベルのDDSであり，いわば蛋白医薬による疾病治療の最適化を目指した"生物学的DDS"と位置づけられる。そこで本技術を用い，TNFR1特異的なアンタゴニストの創出を目的に，TNFの構造変異体ライブラリを網羅的に作製，選別したところ，「TNFR2とは結合せず，TNFR1に対してのみ野生型TNFと同等の結合親和性を示すTNFR1指向性アンタゴニスト(TNF-T2)」を先駆けて創出した(図4)[13,14]。これまで，生理活性蛋白質の構造変異体が野生型蛋白質により発現する生物活性に対してアンタゴニスト活性を示すという概念すらなく，この「蛋白性アンタゴニスト」とも言うべきTNF-T2の創出は，独自に構築した基盤技術を応用することで初めて成し得たものである。さらに，N末端部位特異的に修飾高分子PEGを導入したPEG化TNF-T2(PEG-T2)が，野生型TNF-T2と比較して，*in vitro*におけるアンタゴニスト活性を低下することなく，血中滞留性が飛躍的に増大していることを見出している(図5)。なお，この革新的な部位特異的バイオコンジュゲーション(高分子化学的DDS[15~18])は，前述した生物学的DDSによって機能性リジン欠損蛋白質を創製することで初めて実現可能になるものであり，両基盤技術の融合で，従来法の諸問題の克服に成功したものである。このPEG-T2は，マウスレベルでの実験において，既存の抗TNF蛋白医薬で致命的な問題になっていた宿主の感染防御能の低下を招くことなく，安全に，しかも種々肝炎や関節炎に対して治療効果を発揮すること，その上，いまだ治療薬のない多発性硬化症においても副作用を示すことなく，有効性を発揮することが判明している。すなわち，TNF-T2はTNFR1を介した作用を選択的に阻害することで生体防御機構の破綻を招くことなく，治療効果を発揮できることから，安全かつ有効な自己免疫疾患治療薬となり得ることが示された。現在，TNF-T2のさらなる有用性を評価すべく，他の自己免疫疾患モデルに対しての治療実験

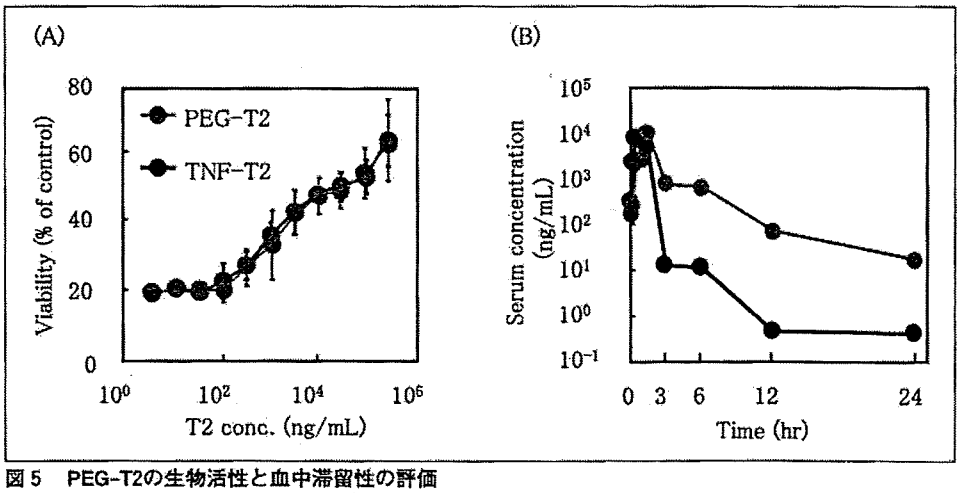

図5 PEG-T2の生物活性と血中滞留性の評価

N末端部位特異的に修飾高分子PEGを導入したPEG-T2のアンタゴニスト活性をL-M assayにて評価した(A)
PEG-T2とT2の血中滞留性の評価は，BALB/cマウスにそれぞれ100ug/mouseで腹腔内投与後，経時的に眼底採血し，ELISAを行った。サンプルごとにスタンダードを作製し，血中濃度を測定した(B)

を進めるとともに，霊長類レベルで医薬品化を目指した研究ステージに移行している。

おわりに

本稿では，創薬プロテオミクス研究から蛋白性医薬品を開発する際の問題点を解決しうる基盤技術の確立に関して紹介した。すなわち，疾患状態で発現変動している疾患関連蛋白質の数が多いため，真に有用な創薬バイオマーカー蛋白質を同定することが困難であった点に関しては，ファージ抗体ライブラリによる*in vitro*抗体作製法をプロテオーム解析に適応した“抗体プロテオミクス技術”を確立し，微量で数多くの発現変動蛋白質をハイスループットにバリデーションすることが可能となった。また，上記で同定した蛋白質の医薬品化に向けた蛋白質固有の問題点である「複数のレセプターを介した多様な生理作用」と「生体内安定性の乏しさ」に対しては，蛋白質そのものに標的指向性を付与する“分子レベルでの生物学的DDS”と機能性人工蛋白質の体内動態制御を可能とする“生体レベルでの高分子化学的DDS”の融合開発が，安全かつ有効な次世代型バイオ医薬品の基盤技術になりうることを示した。現在，抗体医薬をはじめとする蛋白性医薬品が，がんや自己免疫疾患等に対して良好な治療成績をあげており，幅広い分野で新たな蛋白性医薬品の開発が待望されている。今後，産官学が一体となって創薬プロテオミクス研究を推進し，日本発の蛋白性医薬品が数多く上市され，本研究がその一助になればと願っている。

謝辞

本研究では，文部科学省科学研究費補助金特定領域研究(No.20015052)，日本学術振興会科学研究費補助金基盤研究B一般(No.21390046)，厚生労働科学研究費補助金化学物質リスク研究事業(No.H19-化学-一般-005)，厚生労働科学研究費補助金医薬品・医療機器等レギュラトリーサイエンス総合研究事業(No.H19-医薬-一般-010)，厚生労働科学研究費補助金政策創薬総合研究(HS)事業 (No.KHC1017)，厚生労働科学研究費補助金創薬基盤推進研究事業：創薬バイオマーカー探索研究事業(No.H21-バイオ-指定-005)，文部科学省地域科学技術振興施策知的クラスター創成事業，環境省環境研究・技術開発推進費(地球環境研究総合推進費)，厚生労働科学研究費補助金子ども家庭総合研究事業斉(H20-子ども-一般--002)，財団法人永井記念薬学国際交流財団の支援を賜りました。ここに深謝申し上げます。

■参考文献

1) Hanash S.：Nature, **422**, 226-232(2003)
2) Aderka D., H. Engelmann, Y. Maor, C. Brakebusch, and D. Wallach：J Exp Med, **175**, 323-329(1992)
3) Feldmann M., and R. N. Maini：Nat Med, **9**, 1245-1250(2003)
4) Muto Y., K. T. Nouri-Aria, A. Meager, G. J. Alexander, A. L. Eddleston, and R. Williams：Lancet, **2**, 72-74(1988)
5) Breedveld F. C., P. Emery, E. Keystone, K. Patel, D. E. Furst, J. R. Kalden, E. W. St Clair, M. Weisman, J. Smolen, P. E. Lipsky, and R. N. Maini：Ann Rheum Dis, **63**, 149-155(2004)
6) Genovese M. C., J. M. Bathon, R. W. Martin, R. M. Fleischmann, J. R. Tesser, M. H. Schiff, E. C. Keystone, M. C. Wasko, L. W. Moreland, A. L. Weaver, J. Markenson, G. W. Cannon, G. Spencer-Green, and B. K. Finck：Arthritis Rheum, **46**, 1443-1450(2002)
7) Gomez-Reino J. J., L. Carmona, V. R. Valverde, E. M. Mola, and M. D. Montero：Arthritis Rheum, **48**, 2122-2127(2003)
8) Lubel J. S., A. G. Testro, and P. W. Angus：Intern Med J, **37**, 705-712(2007)
9) Sicotte N. L., and R. R. Voskuhl：Neurology, **57**, 1885-1888 (2001)
10) Mori L., S. Iselin, G. De Libero, and W. Lesslauer：J Immunol, **157**, 3178-3182(1996)
11) Kassiotis G., and G. Kollias：J Exp Med, **193**, 427-434(2001)
12) Liu J., M. W. Marino, G. Wong, D. Grail, A. Dunn, J. Bettadapura, A. J. Slavin, L. Old, and C. C. Bernard：Nat Med, **4**, 78-83(1998)
13) Shibata H., Yoshioka Y., Ohkawa A., Minowa K., Mukai Y., Abe Y., Taniai M., Nomura T., Kayamuro H., Nabeshi H., Sugita T., Imai S., Nagano K., Yoshikawa T., Fujita T., Nakagawa S., Yamamoto A., Ohta T., Hayakawa T., Mayumi T., Vandeenabeele P., Aggarwal BB., Nakamura T., Yamagata Y., Tsunoda S., Kamada H., Tsutsumi Y.：J. Biol. Chem., **283**：998-1007, 2008
14) Mukai Y., Shibata H., Nakamura T., Yoshioka Y., Abe Y., Nomura T., Taniai M., Ohta T., Ikemizu S., Nakagawa S., Tsunoda S., Kamada H., Yamagata Y., Tsutsumi Y.：J. Mol. Biol., in press.
15) Kamada H., Tsutsumi Y., Sato-Kamada K., Yamamoto Y., Yoshioka Y., Okamoto T., Nakagawa S., Nagata S., and Mayumi T.：Nat. Biotechnol., **21**：399-404, 2003
16) Yamamoto Y., Tsutsumi Y., Yoshioka Y., Nishibata T., Kobayashi K., Okamoto T., Mukai Y., Shimizu T., Nakagawa S., Nagata S., and Mayumi T.：Nat. Biotechnol., **21**：546-552, 2003
17) Kamada H., Tsutsumi. Y., Yoshioka Y., Yamamoto Y., Kodaiara H., Tsunoda S., Okamoto T., Mukai Y.,Shibata H., Nakagawa S., Mayumi T.：Clin. Cancer Res., **10**(7)：2545-2550, 2004
18) Shibata H., Yoshioka Y., Ikemizu S., Kobayashi K., Yamamoto Y., Mukai Y., Okamoto T., Taniai M., Kawamura M., Abe Y., Nakagawa S., Nagata S., Yamagata Y., Mayumi T., Tsutsumi Y.：Clin. Cancer Res., **10**(24)：8293-8300, 2004.

Int. J. Cancer: **125,** 2316–2322 (2009)

Enhanced expression of Annexin A4 in clear cell carcinoma of the ovary and its association with chemoresistance to carboplatin

Ayako Kim[1,2], Takayuki Enomoto[1], Satoshi Serada[2], Yutaka Ueda[1], Tsuyoshi Takahashi[2,3], Barry Ripley[2], Takashi Miyatake[1], Masami Fujita[1], Chun Man Lee[4], Koji Morimoto[5], Minoru Fujimoto[2], Tadashi Kimura[1] and Tetsuji Naka[2]*

[1]*Department of Obstetrics and Gynaecology, Osaka University Graduate School of Medicine, Osaka, Japan*
[2]*Laboratory for Immune Signal, National Institute of Biomedical Innovation, Osaka, Japan*
[3]*Department of Surgery, Osaka University Graduate School of Medicine, Osaka, Japan*
[4]*Medical Center for Translational Research, Osaka University Hospital, Osaka, Japan*
[5]*Department of Breast and Endocrine Surgery, Osaka University Graduate School of Medicine, Osaka, Japan*

Clear cell carcinoma (CCC) of the ovary is known to be highly resistant to platinum-based chemotherapy. The purpose of our study was to identify a candidate protein that is associated with chemoresistance of CCC and to investigate the specific mechanism of chemoresistance conferred by the identified protein. Enhanced expression of Annexin A4 (Anx A4) was identified in ovarian CCC cells using 2-D differential gel electrophoresis (2D-DIGE) and mass spectrometry. Anx A4 levels were elevated in CCC cells compared with non-CCC cells as determined by real-time RT-PCR and Western blot analysis. Immunohistochemical analysis of Anx A4 was performed in 126 epithelial ovarian cancer tissue samples and demonstrated significantly elevated levels of Anx A4 protein levels in ovarian CCC tumors compared with ovarian serous and endometrioid tumors ($p < 0.01$). Anx A4-transfected ovarian non-CCC cells were more resistant to carboplatin (IC50 = 42 μM) compared with control cells (IC50 = 23 μM) as determined by modified MTT assay. Intracellular platinum levels were significantly lower in Anx A4-transfected cells compared with control cells after carboplatin treatment ($p = 0.0020$) and after an additional 360 min of carboplatin-free incubation ($p = 0.0004$), as measured by atomic absorption spectrophotometry. Expression of Anx A4 is elevated in ovarian CCC tumors and is associated with chemoresistance in cultured ovarian cancer cells. These results demonstrate that Anx A4 confers chemoresistance in ovarian cancer cells in part by enhancing drug efflux. Thus, Anx A4 may represent a novel therapeutic target of chemoresistance in patients with ovarian CCC.

Key words: clear cell carcinoma of the ovary; chemoresistance; Annexin A4

Ovarian cancer is the 5th leading cause of cancer deaths for women in the United States, with approximately 21,600 new cases and 15,500 deaths reported annually.[1] In Japan, it is the eighth most common cause of cancer deaths, with approximately 7,700 new cases (2001) and 4,500 deaths (2007) reported yearly, and the incidence is increasing (Health, Labour and Welfare Ministry, Japan: Population Survey Report). More than 20% of all cases with ovarian cancer in Japan are classified as clear cell carcinoma (CCC) of the ovary, and for unknown reasons, this percentage is markedly higher (by approximately 2-fold) than in Europe and the United States.[2]

Because ovarian cancers (including ovarian CCC) are relatively asymptomatic at early stage, the majority of patients (approximately 70%) present with an advanced stage disease at first diagnosis and subsequently require surgical tumor reduction and adjuvant chemotherapy.[3,4] However, of the 4 major histological types of epithelial ovarian cancer, CCC of the ovary is highly resistant to conventional cancer chemotherapy (including carboplatin and paclitaxel treatment) compared with the other histological types.[2,5,6] Consequently, patients with ovarian CCC are associated with both poorer prognosis and higher mortality than patients with other types of ovarian cancer.[2] Thus, there is an urgent need to further our understanding of the pathogenesis of ovarian CCC, particularly with respect to the expression of proteins, which confer chemoresistance, for the development of a novel therapeutic strategy.

In this study, we performed a proteomic analysis using ovarian cancer cell lines [CCC for comparison with non-CCC serous adenocarcinoma (SAC)] to identify a candidate protein associated with chemoresistance in ovarian CCC. SAC was chosen as a control non-CCC cell line because of its chemosensitivity compared with the chemoresistant CCC cell line. We identified several proteins that are differentially upregulated in ovarian CCC compared with SAC and focused our investigation on Annexin A4 (Anx A4).

Anx A4 is an epithelial isoform of a ubiquitous family of soluble cytoplasmic proteins, which bind to and polymerize on the surface of cell membranes in response to increases in intracellular calcium.[7–9] Although the functions of Anx A4 have not been completely characterized, previous studies have identified major involvement of this protein in membrane permeability,[10] exocytosis[11,12] and regulation of ion channels.[13] Its roles in membrane fluidity and membrane trafficking may in part explain the involvement of Anx A4 in modulating drug resistance in cancer cells.

A previous report associating Anx A4 with chemoresistance in human cancer cell lines focused on human lung and colon cancer cell lines[14] but did not examine ovarian cancer cell lines. In addition, the mechanism of chemoresistance induced by Anx A4 has not been explored in detail. In the study of Morita *et al.*,[15] proteomic analysis showed enhanced expression of Anx A4 in the OVISE and OVTOKO ovarian CCC cell lines compared with the MCAS ovarian mucinous cancer cell line. However, a possible association between Anx A4 expression and chemoresistance was not investigated. Importantly, neither study tried to determine whether Anx A4 protein levels are elevated in tumors of patients with ovarian CCC.

In this study, we have addressed 2 important questions concerning Anx A4 and chemoresistance, *i.e.*, whether expression of Anx A4 is elevated in patient ovarian CCC tumors and by what mechanism Anx A4 confers chemoresistance.

Material and methods

Patients

We examined surgically obtained tumor tissue samples of 126 ovarian cancer patients (Table I) who underwent surgery at Osaka University Hospital, Japan, between 1999 and 2006. None of the patients entered in this study had received adjuvant chemotherapy, including paclitaxel or carboplatin treatment. Histologic features of the tissues were reviewed by board-certified pathologists. Diagnosis was based on the FIGO (International Federation of Gynecologists &

Grant sponsor: Japanese Ministry of Education, Science, Culture and Sports (Grants-Aids for Scientific Research).
***Correspondence to:** Laboratory for Immune Signal, National Institute of Biomedical Innovation, 7-6-8 Saito-asagi, Ibaraki, Osaka 567-0085, Japan. Fax: +81-72-641-9837. E-mail: tnaka@nibio.go.jp
Received 13 February 2009; Accepted after revision 12 May 2009
DOI 10.1002/ijc.24587
Published online 20 May 2009 in Wiley InterScience (www.interscience.wiley.com).

Publication of the International Union Against Cancer
UICC global cancer control

TABLE I - SUMMARY OF CLINICAL CHARACTERISTICS OF OVARIAN CANCER PATIENTS EXAMINED IN THIS STUDY

Histology	Mean age (range)	FIGO stages				Total
		I	II	III	IV	
CCC	53 (36–66)	27	5	9	2	43
Endometrioid	53 (28–66)	2	7	4	0	13
Mucinous	53 (28–90)	6	1	1	0	8
SAC	55 (33–81)	9	13	35	5	62
						126

Obstetricians) classification system. Patient profiles (age, FIGO stage) were analyzed against each of the 4 major epithelial ovarian cancer histological types (CCC, endometrioid adenocarcinoma, mucinous adenocarcinoma and serous adenocarcinoma). Written informed consent was obtained for all the cases, and the experimental protocol was approved by the ethics committee of Osaka University.

Cell lines

Human clear cell carcinoma (CCC) ovarian cancer cell lines (OVISE, OVTOKO, OVMANA and RMG-1) and serous adenocarcinoma (SAC) ovarian cancer cell lines (OVSAHO and OVKATE) were obtained from the Japanese Collection of Research Bioresources (JCRB, Osaka, Japan). Cells were maintained in RPMI 1640 medium supplemented with 10% fetal bovine serum (FBS) (HyClone Laboratories, Logan, UT) and 1% penicillin–streptomycin (Nacalai Tesque, Kyoto, Japan) at 37°C under a humidified atmosphere of 5% CO_2.

Protein extraction and 2D-DIGE

Proteins extracts of the cell lines were prepared with the Complete Mammalian Proteome Extraction Kit (Calbiochem, La Jolla, CA) and stored at −80°C until use. Protein concentrations were determined with the RC-DC Protein Assay kit (Bio-Rad Laboratories, Hercules, CA) using BSA as the standard. Before 2D-DIGE, we performed fluorescence labeling, for which the OVISE and OVSAHO samples were labeled with Cy3 and Cy5 CyDye DIGE fluorminimal dyes (GE Healthcare Bio-Sciences, Little Chalfont, Buckinghamshire, UK), respectively. For first-dimension separation, isoelectric focusing electrophoresis was performed using ReadyStrip™ (Bio-Rad Laboratories) IPG strips (24 cm, pH3-10NL). The labeled proteins (150 μg) were then loaded onto a gel strip, which was rehydrated in the dark for 12 hr (99,000 Vh) with the labeled protein sample diluted to 430 μl with a rehydration buffer (7 M urea, 2 M thiourea, 4% CHAPS, 2 mM TBP, 0.0002% BPB, 1.0% Bio-lyte 3-10 and 1.2% destreak). After isoelectric focusing, proteins were reduced in an equilibration buffer (50 mM Tris-HCl containing 6 M urea, 20% v/v glycerol and 2% SDS, pH 8.8) containing 20 mg/ml DTT for 40 min followed by carbamidomethylation in the equilibration buffer containing 25 mg/ml iodoacetamide for 30 min in the dark. The second-dimension separation was performed on 10% polyacrylamide gels using the Ettan-Dalt-Six system (GE Healthcare Bio-Sciences) at a constant wattage of 100 W at 20°C for 3 hr. Gel electrophoresis was performed in the dark, and the gels were scanned with the Typhoon scanner (GE Healthcare Bio-Sciences).

Protein identification by mass spectrometry

2D-PAGE was performed in parallel with 2D-DIGE using OVISE and OVSAHO protein extracts without fluorescence labeling. Gels were stained using a Silver Stain MS Kit (WAKO Pure Chemical Industries, Ltd., Osaka, Japan). Protein spots in a silver-stained gel, corresponding to the spots of interest in the 2D-DIGE scanned image, were digested in gel according to a previously described method,[16] using sequencing grade modified trypsin (Promega, Inc., Madison, WI). Digested peptides were then extracted with 5% TFA in acetonitrile (ACN/DW 50:45), sonicated for 5 min and concentrated by evaporation. The peptides were solubilized with 0.1% TFA in ACN/DW (2:98) and analyzed by means of LC-MS/MS. For reverse-phase separations, a Magic 2002 capillary HPLC (Michrom BioResources, Auburn, CA) with a C-18 RP column (length 15 cm, i.d. 200 μm; GL Sciences Inc., Tokyo, Japan) was used. The injected peptides were then eluted with a 30-min linear gradient of 5–65% of solvent B (solvent A: 0.1% formic acid in ACN/DW, 2:98; solvent B: 0.1% formic acid in ACN/DW, 95:5). The column was directly interfaced to an LCQ ion trap mass spectrometer (ThermoElectron, San Jose, CA) equipped with a nanoelectrospray ion source, and data were collected in the double mode that was configured to alternate between a single full MS scan and an MS/MS scan of the most intense precursor masses. MS/MS spectra were searched against the human protein Swiss-Prot database with the aid of the MASCOT search program (version 2.1.03; Matrix Science K.K., Tokyo, Japan). The following parameters were used for the search: enzyme: trypsin, missed cleavage; 1, variable modification; oxidation of methionines, fixed modification; carbamidomethylation of cysteins and monoisotopic peptide masses.

Real-time RT-PCR

For the quantification of Anx A4 mRNA in different ovarian cancer cell lines (CCC and SAC), we performed real-time RT-PCR. Total RNA was prepared from OVISE, OVTOKO, OVMANA, RMG-1 (CCC), OVSAHO and OVKATE (SAC) cell lines using an RNeasy Kit (Qiagen Valencia, CA) and cDNA was synthesized with a SuperScript™ III Reverse Transcriptase Kit (Invitrogen, Carlsbad, CA). A standard curve for Anx A4 cDNA was generated by the serial dilution of plasmid vector DNA, which encodes the Anx A4 gene. The primer sequences for Anx A4 were as follows: forward primer, 5′-ggaggtactgtcaaagctgc-3′ and reverse primer, 5′-gccactcagttctgacttcag-3′. Primers and cDNA were added to SYBR green premix (Invitrogen), which contained all the reagents required for PCR. The PCR conditions consisted of 1 cycle at 95°C for 1 min and 42 cycles of 95°C for 20 sec, 50°C for 20 sec and 72°C for 30 sec. PCR products were measured continuously with the My IQ™ Single-Color Real-Time Detection System (Bio-Rad Laboratories).

Western blotting

Cells and frozen tumor tissue samples were lysed in RIPA buffer (10 mM Tris-HCl, pH 7.5, 150 mM NaCl, 1% Nonidet P-40, 0.1% sodium deoxycholate, 0.1% SDS, 1 mM Na_3VO_4 and 1 × protease inhibitor cocktail (Nakalai Tesque)) followed by centrifugation (13,200 rpm, 4°C, 15 min), after which the supernatants were stored at −80°C until use. Protein concentrations were determined with the DC Protein Assay kit (Bio-Rad Laboratories), using BSA as the concentration standard. Extracted proteins were then resolved using 10% Bis-Tris Criterion XT Precast gels (Bio-Rad Laboratories) and subsequently transferred to PVDF membranes (Millipore, Bedford, MA). The membranes were washed and blocked with 1% skim milk in PBS containing 0.1% Tween 20 (PBST) and incubated with a goat polyclonal anti-Anx A4 antibody (sc-1930; Santa Cruz Biotechnology, Santa Cruz, CA) at a 1:300 dilution. Next, the membranes were incubated with horseradish peroxidase-conjugated donkey anti-goat IgG (Santa Cruz Biotechnology). Finally, the signals were visualized by means of an enhanced chemiluminescence (ECL) reaction system (Perkin-Elmer Life Sciences, Boston, MA). For loading control, western blotting and the subsequent antigen–antibody reaction were performed with GAPDH (Santa Cruz Biotechnology).

Immunohistochemistry

Expression of Anx A4 protein in ovarian cancer patient tissue sections was immunohistochemically measured with the ABC Kit (Vector Laboratories, Burlingame, CA). The total number of tissue section samples analyzed was 126 (43 CCC, 13 endometrioid, 8 mucinous, 62 SAC). Sections (3 μm) were prepared from formalin-fixed, paraffin-embedded tissue specimens, deparaffinized and rehydrated in graded alcohols. For antigen retrieval, the sections were incubated in a target retrieval solution (DAKO, Kyoto,

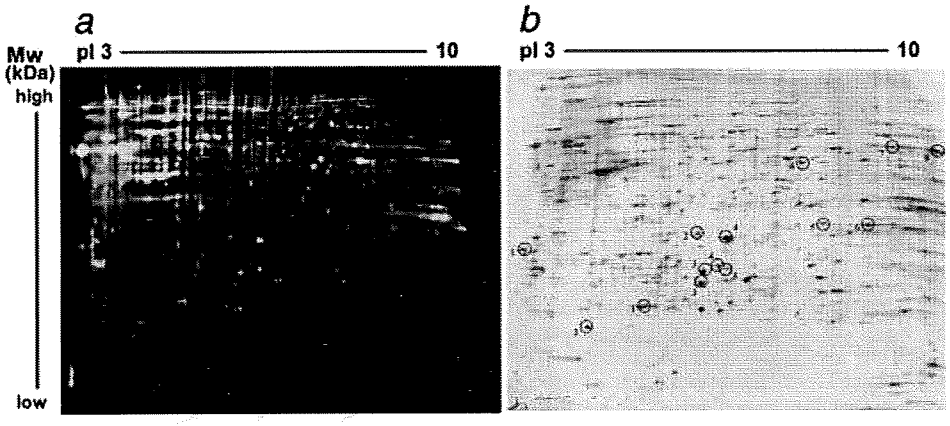

FIGURE 1 – Proteomic analysis of OVISE CCC and OVSAHO SAC cell lines. Representative gel images of 3 independent experiments are shown. A 2D-DIGE gel image of OVISE CCC and OVSAHO SAC cell lines is shown in (*a*). Green spots correspond to proteins upregulated in OVISE cells (Cy3 labeled) compared with OVSAHO cells (Cy5 labeled). Red spots correspond to proteins upregulated in OVSAHO cells (Cy5 labeled) compared with OVISE cells (Cy3 labeled). Yellow spots correspond to proteins expressed at the same level in the OVISE and OVSAHO cell lines. A corresponding silver stain gel image is shown in (*b*).

Japan) in a hot water bath at 98°C for 40 min. In brief, quenching endogenous peroxidase with 3% H_2O_2 in methanol for 20 min. After treatment with BlockAce (Dainippon Sumitomo Pharmaceutical, Osaka, Japan) for 30 min at room temperature, the sections were incubated with a goat polyclonal anti-Anx A4 antibody at 1:100 dilution at 4°C overnight and subsequently incubated with a biotinylated anti-goat IgG antibody (Vector Laboratories Inc.) at room temperature for 1 hr. The antibody complex was detected by incubation with an avidin-biotin-peroxidase complex solution (Vector Laboratories Inc.) and visualized with 3,3′-diaminobenzidine tetrahydrochloride (MERCK, Darmstadt, Germany). Tissue sections were counter-stained with hematoxylin. Three gynecologic oncologists (A.K., T.M., Y.U.), blinded to the histological data, reviewed the stained sections. Cases with >90% of tumor cells staining positively with the anti-Anx A4 antibody were considered strongly positive (+++), cases with >50% but <90% Anx A4-positive cells medium positive (++), those with <50% positive cells weakly positive (+) and those with no or hardly any positive cells were considered negative.

Construction of Anx A4 expression vector

Total RNA from OVISE cells was purified with an RNA-Bee solution (Tel-Test Inc., Friendswood, TX) and cDNA was prepared with a SuperScript™ III Reverse Transcriptase Kit (Invitrogen). To construct the Anx A4 expression vector, cDNA of human Anx A4 was amplified using KOD-plus (Toyobo Co. Ltd., Osaka, Japan) with the following primers: Anx A4 forward primer 5′-ttgacctagagtcatggcca-3′ and Anx A4 reverse primer 5′-tttaatcatctcctccacag-3′. The amplified cDNA was then inserted into pcDNA3.1/V5-His-TOPO vector (Invitrogen) and designated pcDNA3.1-Anx A4. The DNA sequence of Anx A4 cDNA inserted into the plasmid was confirmed using the ABI PRISM 3100 Genetic Analyzer (Applied Biosystems, Foster City, USA).

Generation of Anx A4 stable transfectant cells

To generate Anx A4 stable transfectant cells, the OVSAHO cell line was transfected with pcDNA3.1-Anx A4 using Lipofectamine 2000 (Invitrogen) according to the manufacturers' instructions, after which the cells were selected with 500 μg/ml of Geneticin (GIBCO, Invitrogen, Carlsbad, CA). We also transfected empty vector into the OVSAHO cell line using the same procedure described earlier to generate control cells. Stable clones were maintained in 250 μg/ml of Geneticin. Western blot analysis was performed to confirm the levels of Anx A4 expression in Anx A4 transfectant cells and empty vector control cells.

Measurement of IC_{50} values after carboplatin treatment

Anx A4 transfected OVSAHO cells and empty vector control cells were seeded in 96-well plates (3,000 cells/well) (Costar; Corning Inc., Corning, NY) for 24 hr and then exposed to various concentrations (0-150 μM) of carboplatin for 72 hr. The cells were incubated with 10 μl of Cell Counting Kit-8 (Dojindo, Osaka, Japan) in 100 μl RPMI-1640 medium for 3 hr. Absorbance at 450 nm was measured with a microplate reader (Bio-Rad Model 680), and absorbance values were expressed as percentages relative to those for untreated controls, and the concentrations resulting in 50% inhibition of cell growth (IC_{50} values) were calculated.

Measurement of intracellular platinum accumulation

Carboplatin accumulation in Anx A4 transfected cells and control cells was analyzed according to a previously established method[17] with minor modifications. In brief, 1.5×10^6 cells were seeded into a 60-mm tissue culture dish and incubated for 24 hr. The cells were then exposed to 2 mM carboplatin for 60 min at 37°C and washed twice with PBS either immediately or after 360 min of incubation in carboplatin-free RPMI 1640 medium supplemented with 10% FBS (HyClone Laboratories). After whole-cell extracts were prepared, the concentration of intracellular platinum was determined by using a polarized Zeeman atomic absorption spectrophotometer (model Z-8000; Hitachi, Ltd., Tokyo, Japan). The absolute concentration of platinum in each sample was determined from a calibration curve prepared with a platinum standard solution.

Statistical analysis

Student's *t* tests were used for statistical analyses. For the immunohistochemical analysis, a nonparametric analysis (the Kruskal–Wallis test) was used. A value of $p < 0.05$ was considered statistically significant.

Results

Anx A4 expression is elevated in CCC cell lines compared with SAC cell lines

The protein expression profiles of OVISE (CCC) and OVSAHO (SAC) cell lines were compared by means of 2D-DIGE analyses using fluorminimal dye-labeled protein extracts. The resulting gel images and corresponding silver-stained gels are shown in Figures 1*a* and 1*b*. Eight proteins highly expressed in OVISE cells and 6 proteins in OVSAHO cells were selected for identification by LC-MS/MS analysis. The results of these analyses (Table II) revealed

TABLE II – PROTEINS DIFFERENTIALLY EXPRESSED IN OVISE AND OVSAHO CELL LINES

Spot no.	Access. no.	Identified protein	M_w (Da)	pI	Coverage (%)
Proteins upregulated in OVISE cells compared with OVSAHO cells					
1	P09211	Glutathione S-transferase P	23,438	5.44	38
2	P09525	Annexin A4 (Annexin IV)	35,957	5.85	49
3	P04792	Heat-shock protein beta-1	22,826	5.98	39
4	Q13011	Delta3,5-delta2,4-dienoyl-CoA isomerase, mitochondrial precursor	36,136	8.16	28
5	P30040	Endoplasmic reticulum protein ERp29 precursor	29,032	6.77	15
6	O75874	Isocitrate dehydrogenase [NADP] cytoplasmic	46,915	6.53	39
7	P68104	Elongation factor 1-alpha 1	50,451	9.1	14
8	P68104	Elongation factor 1-alpha 1	50,451	9.1	19
Proteins upregulated in OVSAHO cells compared with OVISE cells					
1	Q07021	Complement component 1 Q subcomponent-binding protein, mitochondrial precursor	31,742	4.74	14
2	O75947	ATP synthase D chain, mitochondrial	18,405	5.22	41
3	P30084	Enoyl-CoA hydratase, mitochondrial precursor	31,823	8.34	27
4	P42126	3,2-trans-enoyl-CoA isomerase, mitochondrial precursor	33,080	8.8	10
5	P45880	Voltage-dependent anion-selective channel protein 2	38,639	6.32	25
6	P45880	Voltage-dependent anion-selective channel protein 2	38,639	6.32	25

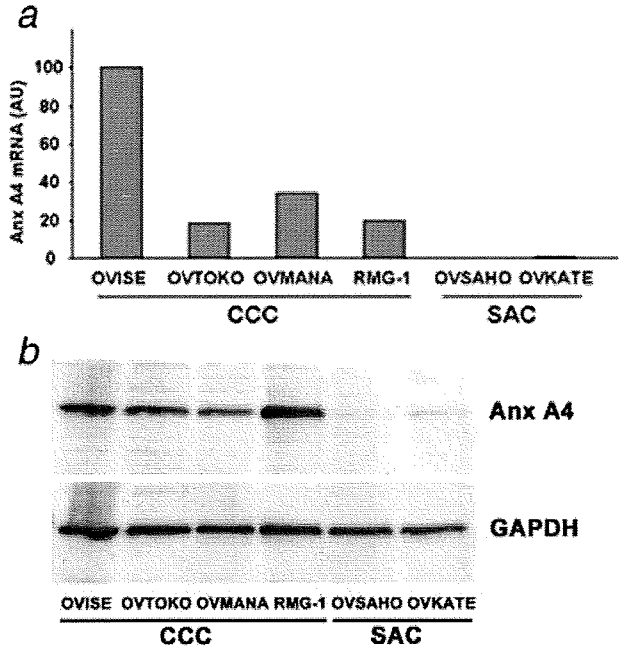

FIGURE 2 – Real-time RT-PCR and Western blot analysis of levels of Annexin A4 expression in ovarian cancer cell lines. Levels of Annexin A4 mRNA in ovarian CCC cell lines (OVISE, OVTOKO, OVMANA and RMG-1) and in ovarian SAC cell lines (OVSAHO and OVKATE) were determined by real-time RT-PCR (*a*). Levels of Annexin A4 protein in ovarian CCC cell lines (OVISE, OVTOKO, OVMANA and RMG-1) and in ovarian SAC cell lines (OVSAHO and OVKATE) were determined by Western blot analysis (*b*).

enhanced expression of the Anx A4 protein in the OVISE cell line compared with the OVSAHO cell line.

The specific overexpression of Anx A4 in ovarian CCC cell lines compared with that in SAC cell lines was further evaluated by real-time RT-PCR (Fig. 2*a*) and Western blot analysis (Fig. 2*b*). As shown in Figure 2*a*, expression of Anx A4 (mRNA level) in OVISE, OVTOKO, OVMANA and RMG-1 (CCC) cell lines was enhanced compared with the OVSAHO and OVKATE (SAC) cell lines where Anx A4 expression (mRNA level) was barely detectable. Western blot analysis (Fig. 2*b*) also demonstrated enhanced expression of Anx A4 (protein level) in OVISE, OVTOKO, OVMANA, RMG-1 (CCC) cell lines compared with the OVSAHO and OVKATE (SAC) cell lines.

Enhanced expression of Anx A4 protein in tumors of ovarian CCC patients

Next, we determined whether levels of Anx A4 protein are elevated in tumors of patients with ovarian CCC compared with other ovarian cancers. For this analysis, we performed an immunohistochemical study of Anx A4 expression in tumor tissue samples from a large cohort of ovarian cancer patients (126 patients in total). In addition, we performed Western blot analysis using several frozen tumor tissue samples and compared the results with those of the immunohistochemical study. Representative immunohistochemical staining of Anx A4 in tissue sections from patients with ovarian cancer revealed intense Anx A4 staining in ovarian CCC compared with other histological types (Fig. 3*a*). Positive staining scores for Anx A4 in tissue sections from patients with other types of ovarian cancers are shown in Figure 3*b*. We observed significantly stronger ($p < 0.01$) positive staining in tissue sections from patients with ovarian CCC compared with patients with ovarian endometrioid and serous adenocarcinoma. Of 43 CCC tissue sections, more than 30 were strongly positive for Anx A4 (+++) compared with only 5 of the 62 SAC samples. Western blot analysis showed enhanced expression of Anx A4 in CCC tumor samples that had demonstrated strong Anx A4 immunohistochemical staining (+++) but barely detectable expression of Anx A4 in SAC tumor samples that had demonstrated negative (−) Anx A4 immunohistochemical staining (Fig. 3*c*).

Transfection of Anx A4 cDNA into ovarian cancer cells enhances resistance to carboplatin treatment and modulates drug cellular efflux

Because Anx A4 has been demonstrated to perform a functional role in chemoresistance in some cancer cell lines,[14] we determined whether Anx A4 can also confer chemoresistance to epithelial ovarian cancer cells. For this study, we generated Anx A4 stably transfected OVSAHO cells. Figure 4*a* shows a Western blot analysis of Anx A4 levels in OVSAHO parent cells, Anx A4 stably transfected OVSAHO cells and empty vector transfected control cells. Figure 4*b* shows cell survival plots for control and OVSAHO/Anx A4 cell lines after treatment with increasing concentrations of carboplatin (0–150 μM). From this analysis, we determined the IC_{50} carboplatin concentration values for the 2 cell lines. Higher (approximately double) IC_{50} carboplatin concentration was observed in the OVSAHO/Anx A4 (IC_{50} = 42 μM) cells compared with the empty vector control cells (IC_{50} = 23 μM). These results demonstrate that Anx A4 can confer chemoresist-

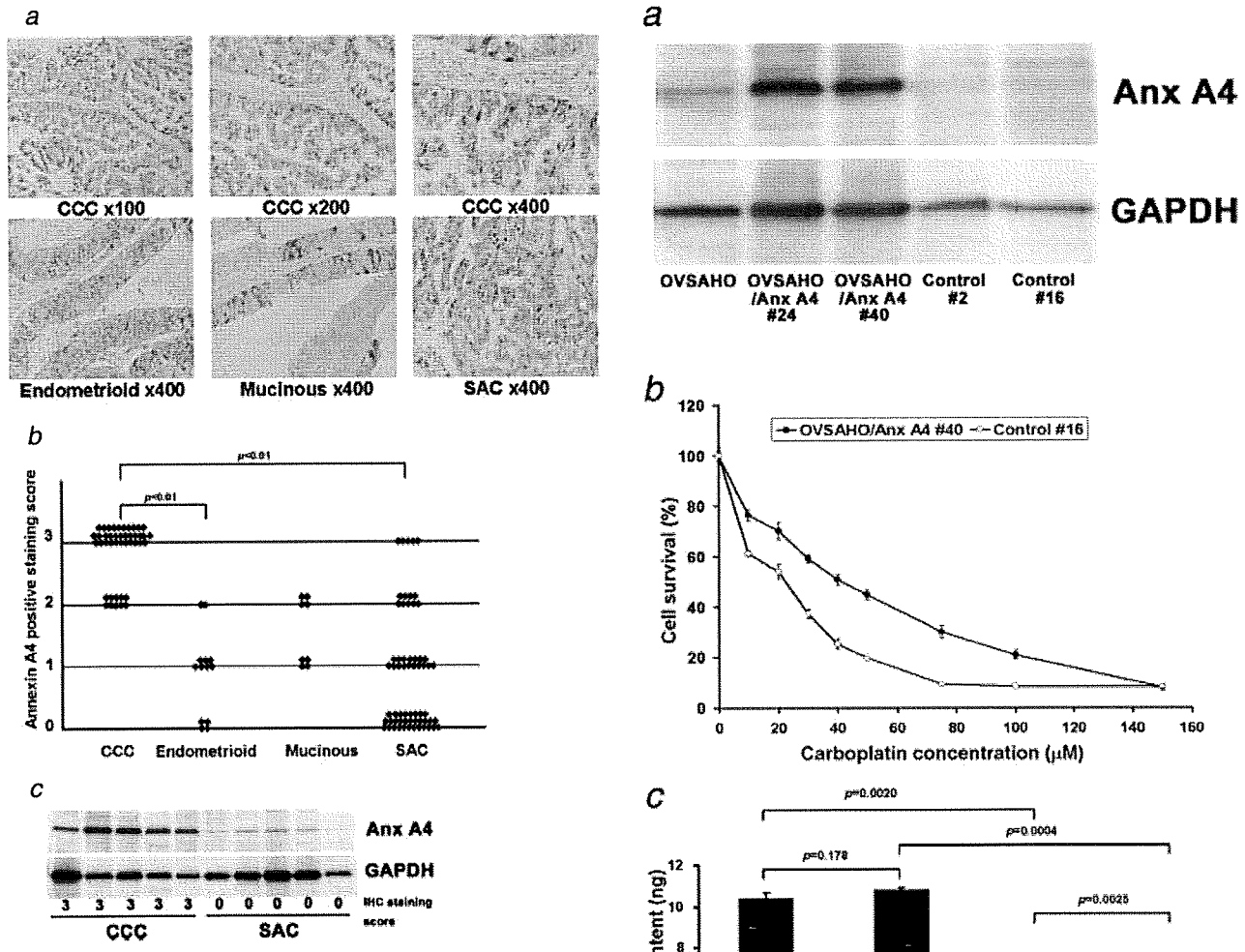

FIGURE 3 – Immunohistochemical analysis of Annexin A4 in ovarian cancer tumors. Levels of Annexin A4 protein in 126 epithelial ovarian cancer samples were determined by immunohistochemical analysis. Representative images of tissue sections from CCC (n = 43), endometrioid (n = 8), mucinous (n = 13) and serous adenocarcinoma (n = 62) ovarian cancer patients after immunohistochemical staining for Annexin A4 (*a*). Annexin A4-positive staining scores of tissue sections from ovarian cancer tumors (*b*). The p value between CCC and SAC is provided as determined by the nonparametric Kruskal–Wallis test. Western blot analysis using 5 CCC frozen tumor samples and 5 SAC frozen tumor samples (*c*).

FIGURE 4 – Transfection of Annexin A4 cDNA into ovarian cancer cells confers resistance to carboplatin and decreases intracellular Pt accumulation. Cell survival (expressed as a percentage relative to control untreated cells) after 72 hr treatment of OVSAHO/Anx A4 and empty vector control cells with different concentrations of carboplatin (Figure 4*a*). The obtained IC50 values were 42 μM for OVSAHO/Anx A4 no. 40 and 23 μM for Control no. 16 (not shown in figure). Intracellular platinum content after treatment with 2 mM carboplatin for 60 min with or without after 360 min of incubation in carboplatin-free medium in OVSAHO/Anx A4 cells and control cells, as determined by atomic absorption spectrophotometry (Figure 4*c*).

ance in ovarian cancer cells. To investigate the molecular mechanisms of chemoresistance induced by Anx A4, we quantitated the intracellular platinum content after treatment of OVSAHO/Anx A4 and empty vector control cells with carboplatin. Figure 4*c* shows an analysis of intracellular platinum accumulation in OVSAHO/Anx A4 cells and empty vector control cells after carboplatin treatment with or without an additional incubation time (360 min) in carboplatin-free medium. Significantly (p = 0.0020) reduced levels of intracellular platinum accumulation were noted in OVSAHO/Anx A4 cells (OVSAHO/Anx A4 no. 40, 0 min) compared with empty vector control cells (Control no. 16, 0 min) when neither cell line underwent additional incubation in carboplatin-free medium. Control cells displayed no significant difference (p = 0.178) in intracellular platinum content between 0 min and 360 min of additional carboplatin-free incubation time (Control no. 16, 0 min *vs.* Control no. 16, 360 min), whereas OVSAHO/Anx A4 cells showed a significant decrease (p = 0.0025) in intracellular platinum content at 360 min as compared with at 0 min of additional carboplatin-free incubation time (OVSAHO/Anx A4 no. 40, 0 min *vs.* OVSAHO/Anx A4 no. 40, 360 min). Furthermore, OVSAHO/Anx A4 cells displayed significantly decreased (p = 0.0004) levels of intracellular platinum con-

tent compared with control cells after an additional 360 min of carboplatin-free incubation (Control no. 16, 360 min *vs.* OVSAHO/Anx A4 no. 40, 360 min), which suggests a role for Anx A4 in enhancing cellular platinum efflux.

Discussion

The use of carboplatin and paclitaxel for the treatment of ovarian cancers has significantly improved survival rates in patients with this disease.[18] However, of the 4 major histological types of ovarian cancer, CCC of the ovary is characterized by strong chemoresistance.[2] Consequently, patients with this disease are associated with significantly lower 5-year survival rates than patients with other histological types of ovarian cancer.[19,20] However, the molecular mechanisms of chemoresistance in this disease have remained poorly understood. Thus, the identification of proteins which are involved in chemoresistance in ovarian CCC is of major clinical importance because these proteins may constitute novel therapeutic targets in this disease.

In this study, we performed a 2D-DIGE proteomic analysis using ovarian cancer cell lines for the identification of a candidate protein associated with chemoresistance in ovarian CCC. We identified 8 proteins differentially upregulated in OVISE CCC cells compared with OVSAHO SAC cells (Table II). From among those 8 proteins, we focused on Anx A4, a calcium-dependent phospholipid-binding protein, which is localized proximal to the cell membrane and plays an important role in membrane fluidity or trafficking.[10]

We confirmed by means of both real-time RT-PCR (mRNA levels) and Western blot analysis (protein levels) that expression of Anx A4 was significantly enhanced in ovarian CCC cell lines compared with in non-CCC ovarian cancer cell lines (Figs. 2*a* and 2*b*). The findings of our analysis using ovarian cancer cell lines are in agreement with those of the proteomic study of Morita *et al.*,[15] in which Anx A4 was identified as being differentially upregulated in ovarian CCC cell lines (OVISE and OVTOKO) compared with an ovarian mucinous cancer cell line.

Previous studies have associated Anx A4 protein with chemoresistance. For example, in a study of Han *et al.*,[14] Anx A4 was observed to be elevated in a paclitaxel-resistant human lung cancer cell line and transfection of Anx A4 cDNA into embryonic kidney 293T cells to confer resistance to paclitaxel. Because Anx A4 has been shown to be involved in modulating membrane permeability and membrane trafficking,[10] it is conceivable that this involvement may result in modulation of both cellular drug influx and efflux after chemo-drug treatment. Taken together, these studies suggest that the strong chemoresistance characteristic of human ovarian CCC may be due to enhanced expression of Anx A4. However, it remained unclear whether levels of Anx A4 protein are significantly elevated in tumors of patients with ovarian CCC compared with other histological types.

In the study reported here, we, therefore, performed an immunohistochemical analysis of Anx A4 in tumor tissue samples from 126 patients with epithelial ovarian cancer to determine whether levels of Anx A4 protein are elevated in tumors of patients with ovarian CCC compared with other epithelial ovarian cancers. Because treatment with paclitaxel can enhance Anx A4 expression in cultured cells,[14] all patients examined in this analysis had undergone preliminary diagnosis and had not received chemotherapy (including carboplatin or paclitaxel) before surgery. The results of this analysis revealed significantly ($p < 0.01$) strong positive staining (enhanced expression) of Anx A4 in tumor tissue samples from patients with ovarian CCC compared with endometrioid and serous adenocarcinoma, which are known to represent chemosensitive histological types (Fig. 3*b*). Western blot analysis using frozen tumor samples were compatible with results of the IHC study (Fig. 3*c*). Thus, our study was able to demonstrate the presence of enhanced expression of Anx A4 in tumors of patients with ovarian CCC. This finding is in agreement with that of our proteomic analysis using ovarian cancer cell lines and indicates that Anx A4 may play a role in tumor resistance to cancer chemotherapy in patients with ovarian CCC.

To investigate a relationship between levels of expression of Anx A4 and patient prognosis, we reviewed clinical outcomes (recurrence, progression-free survival, etc.) of the 62 SAC patients including 5 patients with strong (+++)Anx A4 povitive staining in IHC analysis. Among the 5 SAC patients with high levels of Anx A4 expression, 2 patients are well and alive with no recurrence, whereas the other 2 patients have recurred within 1 or 2 years after treatment and 1 patient was out of follow-up. We have compared the progression-free survival between these 5 patients and Anx A4 negative SAC patients and there was no statistically significant difference between the 2 groups. Because the number of Anx A4-positive SAC patients is small, further investigation will be necessary in a larger cohort of patients.

Although previous studies have demonstrated a role for Anx A4 in conferring chemoresistance to human cancer cell lines,[14] a similar role in human epithelial ovarian cancer cells was not identified, and the specific mechanism of chemoresistance that Anx A4 confers was not previously determined. Therefore, we first studied cell survival after carboplatin treatment to confirm whether Anx A4 can enhance chemoresistance in epithelial ovarian cancer cells. We were unable to reduce Anx A4 protein levels in the OVISE CCC cell line, despite using various strategies (including siRNA), which may be due to the reported long half-life of Anx A4 protein (approximately 4 days).[21] We then tested the effect of forced overexpression of Anx A4 in the OVSAHO non-CCC (SAC) ovarian cancer cell line in which Anx A4 is not endogenously expressed. We observed enhanced chemoresistance to carboplatin treatment in cells that stably expressed Anx A4 compared with empty vector control cells (Figs. 4*a* and 4*b*). Thus, our results demonstrate that Anx A4 protein plays a role in the enhancement of chemoresistance in epithelial ovarian cancer cells.

We next examined intracellular platinum accumulation in both Anx A4 expressing ovarian cancer cells (OVSAHO/Anx A4 cells) and empty vector control cells after carboplatin treatment (Fig. 4*c*). Our results of carboplatin treatment with no carboplatin-free incubation revealed significantly reduced levels of intracellular platinum content in OVSAHO/Anx A4 cells compared with control cells, which indicates that Anx A4 inhibits cellular platinum influx and/or promotes cellular platinum efflux. Comparison of the results for 0 and 360 min carboplatin-free incubation showed that OVSAHO/Anx A4 cells are more active in promoting cellular platinum efflux compared with control cells. Taken together, these results demonstrate that Anx A4 plays a part in the enhancement of cellular platinum efflux.

Our study has demonstrated for the first time elevated levels of Anx A4 protein in patients with ovarian CCC and an association between elevated Anx A4 levels and enhanced chemoresistance to carboplatin in human epithelial ovarian cancer cells. It has also found evidence for the first time that Anx A4 confers chemoresistance in part by enhancing drug efflux. Thus, it is conceivable that the observed strong resistance to cancer chemotherapy (including carboplatin) specific to ovarian CCC tumors, compared with that of other epithelial ovarian tumors, is mediated through the enhanced expression of Anx A4 in patients with this disease. Therefore, Anx A4 may constitute a novel therapeutic target for overcoming resistance to cancer chemotherapy in patients with ovarian CCC. In view of the reported half-life of Anx A4 protein, such a therapeutic strategy is likely to involve the inhibition of the function rather than of the expression of Anx A4 in patients with CCC.

Acknowledgements

The authors are grateful for experimental assistance from Ms. Y. Matsukawa and for secretarial assistance from Ms. Y. Ito and Ms. N. Kawakami.

References

1. Jemal A, Siegel R, Ward E, Hao Y, Xu J, Murray T, Thun MJ. Cancer statistics, 2008. CA Cancer J Clin 2008;58:71–96.
2. Itamochi H, Kigawa J, Terakawa N. Mechanisms of chemoresistance and poor prognosis in ovarian clear cell carcinoma. Cancer Sci 2008; 99:653–8.
3. Jacobs IJ, Menon U. Progress and challenges in screening for early detection of ovarian cancer. Mol Cell Proteomics 2004;3:355–66.
4. Rapkiewicz AV, Espina V, Petricoin EF, III, Liotta LA. Biomarkers of ovarian tumours. Eur J Cancer 2004;40:2604–12.
5. Sugiyama T, Kamura T, Kigawa J, Terakawa N, Kikuchi Y, Kita T, Suzuki M, Sato I, Taguchi K. Clinical characteristics of clear cell carcinoma of the ovary: a distinct histologic type with poor prognosis and resistance to platinum-based chemotherapy. Cancer 2000;88: 2584–9.
6. Pectasides D, Pectasides E, Psyrri A, Economopoulos T. Treatment issues in clear cell carcinoma of the ovary: a different entity? Oncologist 2006;11:1089–94.
7. Kaetzel MA, Hazarika P, Dedman JR. Differential tissue expression of three 35-kDa annexin calcium-dependent phospholipid-binding proteins. J Biol Chem 1989;264:14463–70.
8. Zanotti G, Malpeli G, Gliubich F, Folli C, Stoppini M, Olivi L, Savoia A, Berni R. Structure of the trigonal crystal form of bovine annexin IV. Biochem J 1998;329:101–6.
9. Kaetzel MA, Mo YD, Mealy TR, Campos B, Bergsma-Schutter W, Brisson A, Dedman JR, Seaton BA. Phosphorylation mutants elucidate the mechanism of annexin IV-mediated membrane aggregation. Biochemistry 2001;40:4192–9.
10. Hill WG, Kaetzel MA, Kishore BK, Dedman JR, Zeidel ML. Annexin A4 reduces water and proton permeability of model membranes but does not alter aquaporin 2-mediated water transport in isolated endosomes. J Gen Physiol 2003;121:413–25.
11. Sohma H, Creutz CE, Gasa S, Ohkawa H, Akino T, Kuroki Y. Differential lipid specificities of the repeated domains of annexin IV. Biochim Biophys Acta 2001;1546:205–15.
12. Piljic A, Schultz C. Annexin A4 self-association modulates general membrane protein mobility in living cells. Mol Biol Cell 2006;17: 3318–28.
13. Kaetzel MA, Chan HC, Dubinsky WP, Dedman JR, Nelson DJ. A role for annexin IV in epithelial cell function. Inhibition of calcium-activated chloride conductance. J Biol Chem 1994;269:5297–302.
14. Han EK, Tahir SK, Cherian SP, Collins N, Ng SC. Modulation of paclitaxel resistance by annexin IV in human cancer cell lines. Br J Cancer 2000;83:83–8.
15. Morita A, Miyagi E, Yasumitsu H, Kawasaki H, Hirano H, Hirahara F. Proteomic search for potential diagnostic markers and therapeutic targets for ovarian clear cell adenocarcinoma. Proteomics 2006;6: 5880–90.
16. Shevchenko A, Wilm M, Vorm O, Mann M. Mass spectrometric sequencing of proteins silver-stained polyacrylamide gels. Anal Chem 1996;68:850–8.
17. Ikuta K, Takemura K, Sasaki K, Kihara M, Nishimura M, Ueda N, Naito S, Lee E, Shimizu E, Yamauchi A. Expression of multidrug resistance proteins and accumulation of cisplatin in human non-small cell lung cancer cells. Biol Pharm Bull 2005;28:707–12.
18. Paclitaxel plus carboplatin versus standard chemotherapy with either single-agent carboplatin or cyclophosphamide, doxorubicin, and cisplatin in women with ovarian cancer: the ICON3 randomised trial. Lancet 2002;360:505–15.
19. Tammela J, Geisler JP, Eskew PN, Jr, Geisler HE. Clear cell carcinoma of the ovary: poor prognosis compared to serous carcinoma. Eur J Gynaecol Oncol 1998;19:438–40.
20. O'Brien ME, Schofield JB, Tan S, Fryatt I, Fisher C, Wiltshaw E. Clear cell epithelial ovarian cancer (mesonephroid): bad prognosis only in early stages. Gynecol Oncol 1993;49:250–4.
21. Raynal P, Pollard HB, Srivastava M Cell cycle and post-transcriptional regulation of annexin expression in IMR-90 human fibroblasts. Biochem J 1997;322:365–71.

Journal of Cellular Physiology

CDK Inhibitors Selectively Diminish Cell Cycle Controlled Activation of the Histone H4 Gene Promoter by p220^{NPAT} and HiNF-P

PARTHA MITRA,[1] PRACHI N. GHULE,[1] MARGARETHA VAN DER DEEN,[1] RICARDO MEDINA,[1] RONG-LIN XIE,[1] WILLIAM F. HOLMES,[1] XIN YE,[2] KEIICHI I. NAKAYAMA,[3] J. WADE HARPER,[2] JANET L. STEIN,[1] GARY S. STEIN,[1]* AND ANDRE J. VAN WIJNEN[1]*

[1]*Department of Cell Biology and Cancer Center, University of Massachusetts Medical School, Worcester, Massachusetts*

[2]*Department of Pathology, Harvard Medical School, Boston, Massachusetts*

[3]*Department of Molecular and Cellular Biology, Kyushu University, Fukuoka, Japan*

Cell cycle progression into S phase requires the induction of histone gene expression to package newly synthesized DNA as chromatin. Cyclin E stimulation of CDK2 at the Restriction point late in G1 controls both histone gene expression by the p220^{NPAT}/HiNF-P pathway and initiation of DNA replication through the pRB/E2F pathway. The three CDK inhibitors (CKIs) p21$^{CIP1/WAF1}$, p27^{KIP1}, and p57^{KIP2} attenuate CDK2 activity. Here we find that γ-irradiation induces p21$^{CIP1/WAF1}$ but not the other two CKIs, while reducing *histone H4* mRNA levels but not *histone H4* gene promoter activation by the p220^{NPAT}/HiNF-P complex. We also show that p21$^{CIP1/WAF1}$ is less effective than p27^{KIP1} and p57^{KIP2} in inhibiting the CDK2 dependent phosphorylation of p220^{NPAT} at subnuclear foci and transcriptional activation of *histone H4* genes. The greater effectiveness of p57^{KIP2} in blocking the p220^{NPAT}/HiNF-P pathway is attributable in part to its ability to form a specific complex with p220^{NPAT} that may suppress CDK2/cyclin E phosphorylation through direct substrate inhibition. We conclude that CKIs selectively control stimulation of the *histone H4* gene promoter by the p220^{NPAT}/HiNF-P complex.

J. Cell. Physiol. 219: 438–448, 2009.

At the G1/S phase transition of the human cell cycle, DNA replication is initiated and histone gene expression is induced to package nascent DNA. At the restriction point that precedes the G1/S boundary, growth factor dependent signaling pathways activate cyclin E and its cognate cyclin dependent kinase 2 (CDK2) (Blagosklonny and Pardee, 2002; Sherr and Roberts, 2004). Cyclin E/CDK2 complexes control phosphorylation of two distinct regulatory pathways to support the synthesis of DNA or histone proteins. One pathway is initiated by phosphorylation of the retinoblastoma protein pRB(RB1) which releases E2F proteins that stimulate transcription of a number of genes to support the initiation and progression of DNA synthesis during S phase (e.g., *DHFR*, *TK*, *DNA polymerase α*) (Dyson, 1998; Nevins, 2001). Equally important, cyclin E/CDK2 controls the activity of the histone gene transcription factor HiNF-P through phosphorylation of its co-activator p220^{NPAT}, and this complex coordinately regulates *histone H4* gene expression in somatic cells (Pauli et al., 1987; van Wijnen et al., 1992; Ma et al., 2000; Zhao et al., 2000; Mitra et al., 2003, 2007; Holmes et al., 2005; Miele et al., 2005) and human embryonic stem cells (Becker et al., 2006, 2007; Ghule et al., 2007). HiNF-P and p220^{NPAT} co-localize at Cajal Body-related subnuclear foci together with histone genes and factors that support the processing of histone gene transcripts (Ma et al., 2000; Zhao et al., 2000; Shopland et al., 2001; Miele et al., 2005; Ghule et al., 2007). In addition, HiNF-P and p220^{NPAT} are components of broader regulatory networks of protein/protein interaction and target genes involved in cell cycle control (Medina et al., 2006, 2007; Miele et al., 2007; Xie et al., 2007).

CDK2 activity is regulated by direct binding to one of three CDK inhibitory proteins (CKIs) p21$^{CIP1/WAF1}$ (CDKN1A), p27^{KIP1} (CDKN1B), and p57^{KIP2} (CDKN1C) that have distinct biological roles in mammalian development (Harper et al., 1993; el-Deiry et al., 1994; Luo et al., 1995; Matsuoka et al., 1995; Zhang et al., 1997, 1998, 1999; Nakayama and Nakayama, 1998; Reynaud et al., 1999; Sherr and Roberts, 1999). The general roles of p21$^{CIP1/WAF1}$ and p27^{KIP1} in mediating cell cycle arrest during differentiation or DNA damage responses have been extensively investigated, but the function of p57^{KIP2} has been more enigmatic (Baumbach et al., 1987). The expression of *p57^{KIP2}* in vivo is more restricted than that of *p27^{KIP1}* and

Abbreviations: HiNF-P, histone nuclear factor P; CDK, cyclin dependent kinase; NPAT, nuclear protein; ataxia-telangiectasia locus; CIP, CDK inhibitory protein; KIP, kinase inhibitory protein; CKI, CDK inhibitor; PRB, retinoblastoma protein; E2F, adenovirus early gene 2 transcription factor; skp2, S phase kinase associated protein 2; SDS, sodium dodecyl sulfate; PAGE, polyacrylamide gel electrophoresis; PCR, polymerase chain reaction; HPRT, hypoxanthine guanine phosphoribosyl transferase; TK, thymidine kinase; DHFR, dihydrofolate reductase.

Contract grant sponsor: NIH;
Contract grant numbers: GM32010, GM54137, P30 DK32520.

Partha Mitra's present address is Department of Cell Biology, Evolva Biotech (SA), Hyderabad, India.

*Correspondence to: Gary S. Stein and Andre J. van Wijnen, Department of Cell Biology, University of Massachusetts Medical School, 55 Lake Avenue North, Worcester, MA 01655.
E-mail: gary.stein@umassmed.edu and andre.vanwijnen@umassmed.edu

Received 26 November 2008; Accepted 3 December 2008

Published online in Wiley InterScience (www.interscience.wiley.com.), 23 January 2009.
DOI: 10.1002/jcp.21687

$p21^{CIP1/WAF1}$ due to CpG methylation dependent imprinting (Matsuoka et al., 1995, 1996; Kondo et al., 1996). Loss of $p57^{KIP2}$ expression in mice and humans may increase susceptibility to specific tumors (Zhang et al., 1997; Caspary et al., 1999), and the $p57^{KIP2}$ gene is transcriptionally silenced in several cancers (Kikuchi et al., 2002; Li et al., 2002; Canalli et al., 2005; Lodygin et al., 2005). Structural similarities between CKIs (e.g., N-terminal cyclin binding domain) reflect biochemical redundancy in blocking CDK2 and the shared ability to attenuate cell growth and mediate checkpoint control. However, the structure of $p57^{KIP2}$ is distinct, because it contains a C-terminal proline-alanine extension (PAPA repeat) (Matsuoka et al., 1995). While

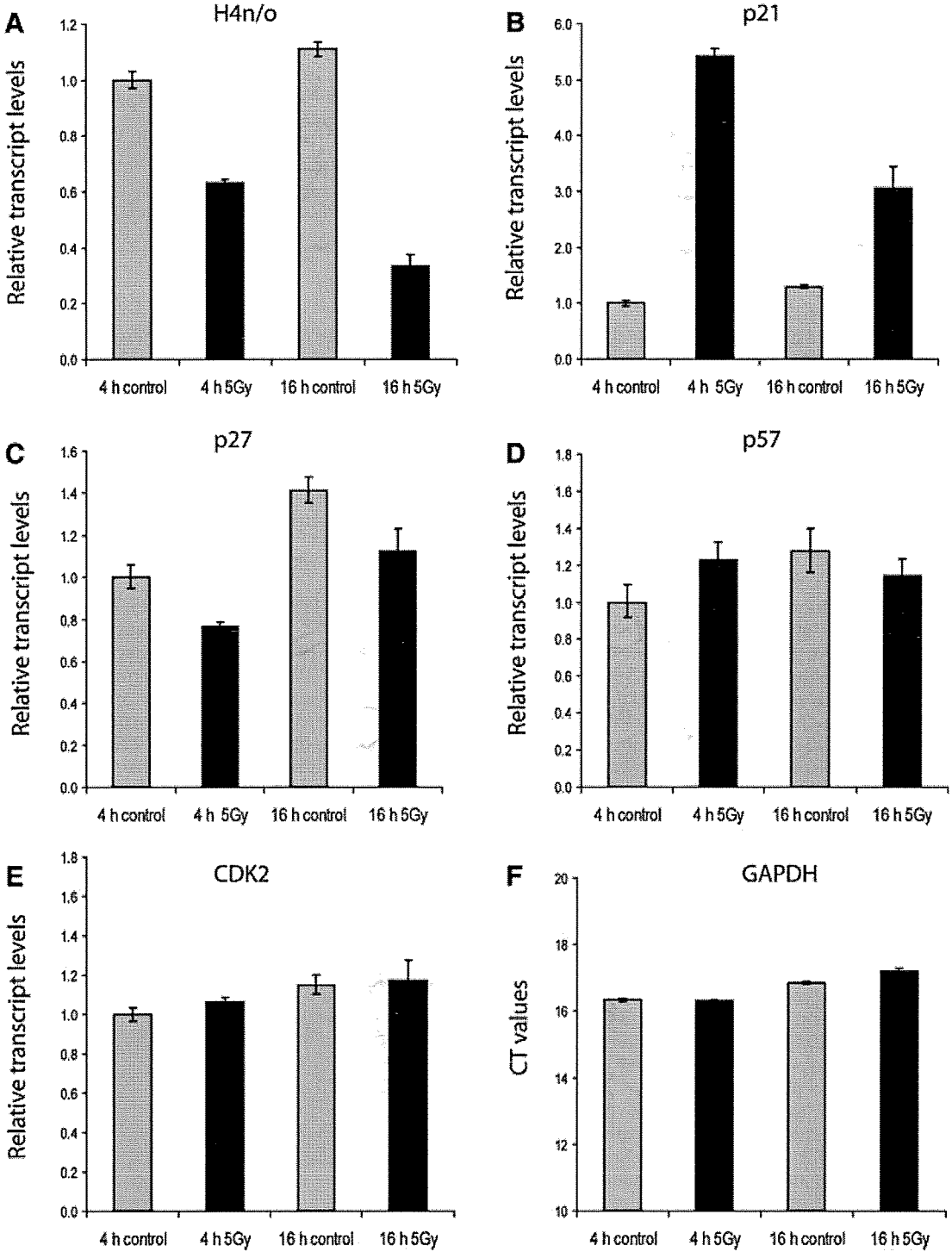

Fig. 1. γ-Irradiation reduces *histone H4* gene expression while selectively modulating the expression of $p21^{CIP1/WAF1}$ and $p27^{KIP1}$. U2OS cells were exposed to 5 Gy irradiation at 24 h after transfection. At 4 or 16 h after irradiation, total RNA was extracted and purified from triplicate experiments. The relative mRNA expression of *H4n* (A), $p21^{CIP1/WAF1}$ (B), $p27^{KIP1}$ (C), $p57^{KIP2}$ (D), and *CDK2* (E) was calculated with the ΔΔCT method using *GAPDH* (F) as an internal control. For *GAPDH*, the CT values were plotted and these values did not change appreciably upon irradiation.

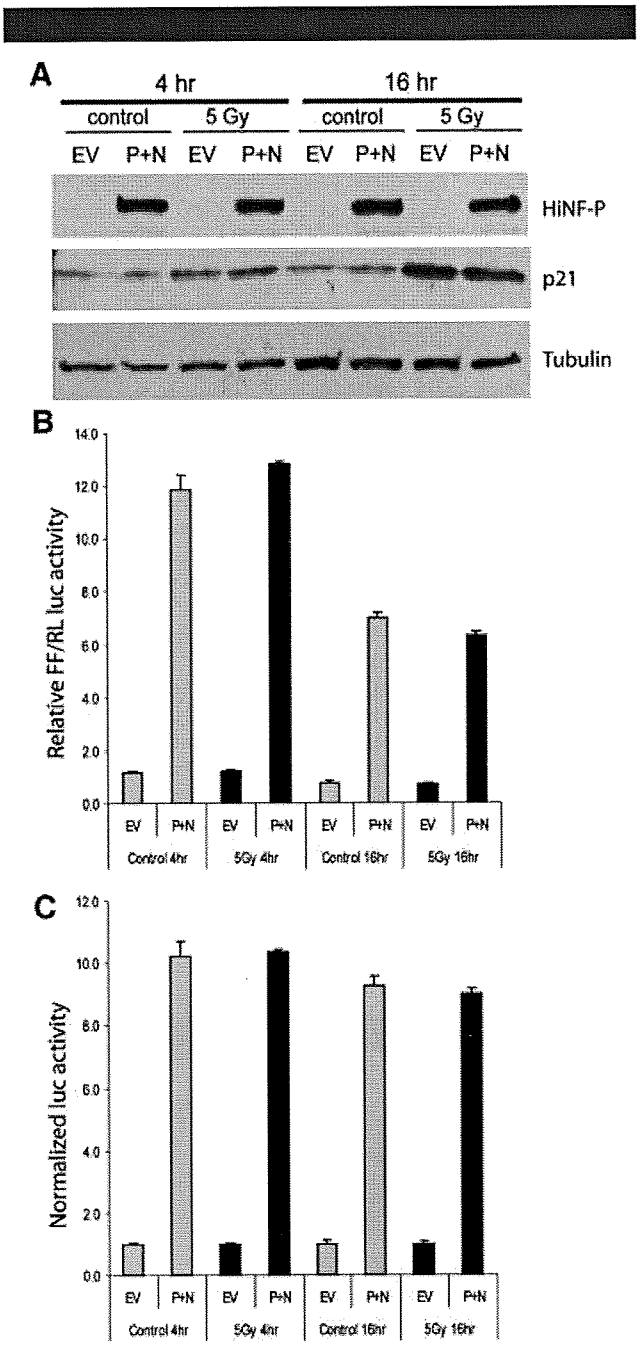

Fig. 2. Co-activation of the *histone H4/n* gene by HiNF-P and $p220^{NPAT}$ occurs independently of γ-irradiation. U2OS cells were transiently transfected with a wild-type *histone H4* promoter luciferase reporter construct and co-transfected with the expression vectors for HiNF-P (P), or $p220^{NPAT}$ (N), or empty expression vector (EV). For irradiation experiments, cells were exposed to 5 Gy at 24 h after transfection. At 4 or 16 h after irradiation, cell lysates were analyzed for (A) protein levels of HiNF-P and $p21^{CIP1/WAF1}$ by Western blotting protein and (B,C) for luciferase activity. Firefly (FF) luciferase activity was normalized to *Renilla* (RL) luciferase activity in part B. In part C, these values are normalized to the empty vector. Error bars indicate standard deviations from triplicate experiments.

all three CKIs can inhibit CDK activity, $p57^{KIP2}$ may have unique properties that have not yet been appreciated.

In this study, we compare the inhibitory function of $p21^{CIP1/WAF1}$, $p27^{KIP1}$, and $p57^{KIP2}$ in the cyclin E/CDK2/$p220^{NPAT}$/HiNF-P/histone gene-regulatory pathway that supports entry into S phase. Our data suggest that CKIs exhibit selectivity in their ability to inhibit signaling at the histone H4 promoter through the $p220^{NPAT}$/HiNF-P complex, a principal CDK2 substrate that operates in parallel to the pRB/E2F pathway at the G1/S phase transition.

Experimental Procedures

Cell culture and transient transfections

Cos7 cells were co-transfected with HiNF-P responsive promoters (i.e., *histone H4*) fused to luciferase reporters and expression vectors encoding the indicated proteins (e.g., $p57^{KIP2}$, $p220^{NPAT}$ and HiNF-P) using FuGENE6 (Mitra et al., 2003; Miele et al., 2005). Luciferase activity was measured within 24 h. Vectors for human Myc-tagged $p57^{KIP2}$ (Roger Watson, Imperial College of London, UK), mouse $p57^{KIP2}$ (James Cross, University of Toronto), mouse $p27^{KIP1}$ (Jack Pledger, University of South Florida, Tampa, Florida) and human Skp2 and a Skp2 F-box deletion mutant (Skp2ΔF), were the generous gifts of the indicated individuals. Adenovirus $p57^{KIP2}$ was kindly provided by Matthew Stewart (University of Illinois).

Treatments with $p57^{KIP2}$ siRNA smart pool duplexes or universal controls (Dharmacon RNA Technologies, Chicago, IL) were performed at 12–16 h after co-transfection of H4/luciferase reporters. At 48 h, we examined luciferase activity using a luminometer and $p57^{KIP2}$ levels by immunoblotting with ~15–20 μg total protein separated by 10% SDS–PAGE (Mitra et al., 2003; Miele et al., 2005). Immunoprecipitations were obtained with ~100 μg of whole cell extract protein, the indicated antibodies and protein A/G-agarose after overnight incubation at 4°C. Samples were then separated by 9% or 10% SDS–PAGE followed by western blotting and chemiluminescence detection.

Expression analysis and reporter gene assays

For reporter gene assays with irradiated cells, we plated U2OS cells at a density of 1.1×10^5 cells per well in six-well plates. The next day, co-transfections were performed using FuGENE6 (Roche) with the same wild-type histone H4 promoter luciferase reporter construct (200 ng) as above and expression vectors for HiNF-P (25 ng) or $p220^{NPAT}$ (200 ng) or the corresponding empty vector as described previously (Mitra et al., 2003; Miele et al., 2005) while maintaining the same total amount of DNA in every transfection. Cells were irradiated by exposure to 5 or 12 Gy γ-irradiation at 24 h after transfection. At 4 or 16 h after irradiation, cell lysates were analyzed for luciferase activity and normalized to *Renilla* (phRL-null, 5 ng per well) using the dual-luciferase reporter assay system (Promega, Madison, WI).

Reporter gene experiments were also performed with normal diploid human WI-38 cells. These cells were plated at a density of 1.6×10^5/well in six-well plates and transiently transfected at day 2 after plating at a cell density of ~30% with wild-type histone H4 promoter luciferase reporter construct, and co-transfected with the expression vectors HiNF-P, $p220^{NPAT}$, or p57 as described above. The same total amount of DNA (2.5 μg) was maintained in every transfection. Lipofectamine LTX (Invitrogen, Carlsbad, CA) was used as a transfection agent in combination with PLUS reagent (Invitrogen) and transfection was performed in the absence of FBS and antibiotics. After 16 h medium was changed to normal growth medium with FBS, and cells were lysed in 1× PLB lysis buffer (Promega) after a total of 40 h transfection time. Cell lysates were analyzed for luciferase activity and normalized to *Renilla* (phRL-null) with dual-luciferase reporter assay system (Promega).

For protein analyses, cell lysates obtained from reporter gene assays were diluted in SDS sample buffer and loaded on a 4–15% ready gel precast gel (Bio-Rad, Hercules, CA). HiNF-P

was detected with the 802 antibody (1:2,000 dilution) (Mitra et al., 2003; Miele et al., 2005) and $p21^{CIP1/WAF1}$ was visualized with a commercially available antibody (sc-756; 1:1,000 dilution, Santa Cruz Biotechnology, Santa Cruz, CA). Tubulin was used as an internal control. Peroxidase labeled goat-anti-rabbit antibody (Santa Cruz) was used as secondary antibody and visualized with enhanced chemiluminescence (ECL) chemistry (PerkinElmer, Waltham, MA).

The levels of mRNAs for human histone *HIST2H4 (H4/n)*, $p21^{CIP1/WAF1}$, $p27^{KIP1}$ and $p57^{KIP2}$, *CDK2*, and *GAPDH* were detected by quantitative real-time reverse transcriptase PCR (qRT-PCR). Purified total RNA using Trizol (Invitrogen) from triplicate experiments of reporter gene assays was subjected to DNase I digestion, and cDNA was prepared with the iScript cDNA synthesis kit (Bio-Rad). Relative quantitation was determined using a 7000 sequence detection system (Applied Biosystems) with SYBR Green chemistry (Applied Biosystems). The relative mRNA expression was calculated with the ΔΔCT method. Real-time primer sequences for *H4/n*, *p27* and *CDK2* were published previously (Becker et al., 2007; Medina et al., 2007). The following primer pairs were used for human mRNA (in 5′–3′ direction): p21 forward 5′-GGA AGA CCA TGT GGA CCT GT and reverse 5′-GGC GTT TGG AGT GGT AGA AA; p57 forward 5′-AAG AGA TCA GCG CCT GAG AA and reverse 5′-TGG GCT CTA AAT TGG CTC AC; GAPDH forward 5′-ATG TTC GTC ATG GGT GTG AA and reverse 5′-TGT GGT CAT GAG TCC TTC CA.

We also examined gene expression in total RNA that was extracted and purified from mouse embryonic fibroblasts (MEFs) isolated from wild type *p57* (WT), heterozygous *p57* null (HET) and homozygous *p57* null (KO) mice. The relative mRNA expression of mouse *HiNF-P*, *Hist2H4*, *HistH4/m and Hist1H4/f*, *p57*, *p27*, and *p21* was calculated using the ΔΔCT method with *HPRT* as an internal control. The following mouse primer sequences were used: p57 forward: 5′-GTC TGA GAT GAG TTA GTT TAG AGG and reverse 5′-TGC TAC ATG AAC GAA AGG TC; p27 forward 5′ TCT AAA GCC CAC TTA TAA CCC AG and reverse 5′-CCT GTG CCA TCT CTA TAT TCC T; p21 forward 5′-CTT CTC CCA TTT CTT AGT AGC AG and reverse 5′-CCA CGG TAT TCA ACA CTG AG; HiNF-P forward 5′-ATG TTT GCC AAC AAC ACC AA and reverse 5′-GCC TCT CTG TGG CAA ATC TC; Hist2h4 forward 5′-CCA GCT GGT GTT TCA GAT TAC A and reverse 5′-ACC CTT GCC TAG ACC CTT TC; Hist1h4m forward 5′-GAG CAG TAC AGT TTT GTC TTC ATC A and reverse 5′-CGT GAT GCC CTG GAT GTT AT; Hist1h4f forward 5′-CAA CTC AGT GCT CCA TAG CC and reverse 5′-GGT GAT GCC CTG GAT GTT AT; Hprt1 forward 5′-CAG GCC AGA CTT TGT TGG AT and reverse 5′-TTG CGC TCA TCT TAG GCT TT.

Immunofluorescence microscopy

Cells grown on gelatin-coated coverslips (Fisher Scientific, Springfield, NJ) were examined by in situ immunofluorescence microscopy 24 h after transfection (Miele et al., 2005). Cells were washed with cold saline, fixed with 3.7% formaldehyde for 10 min on ice, and permeabilized with 0.1% Triton X-100 for 20 min. Coverslips were blocked with serum albumin prior to antibody staining and incubated at 37°C for 1 h with the following antibodies using 1:1,000 dilutions (unless indicated otherwise): mouse Flag (1:10,000; Sigma St. Louis, MO) and $p220^{NPAT}$ (BD Biosciences, San Jose, CA) monoclonals and rabbit polyclonals against phospho-Thr1270 and phospho-Thr1350 of $p220^{NPAT}$ (Ma et al., 2000). Cells were incubated at 37°C for 1 h with Alexa 488 goat anti-rabbit or Alexa 594 goat anti-mouse (Molecular Probes, Eugene, OR). Cells were stained with 4′,6-diamidino-2-phenylindole (DAPI) (5 mg/ml) for 5 min, mounted to slides and examined by an Axioplan 2 epifluorescence microscope (Zeiss, Thornwood, NY) attached to a charge-coupled device camera.

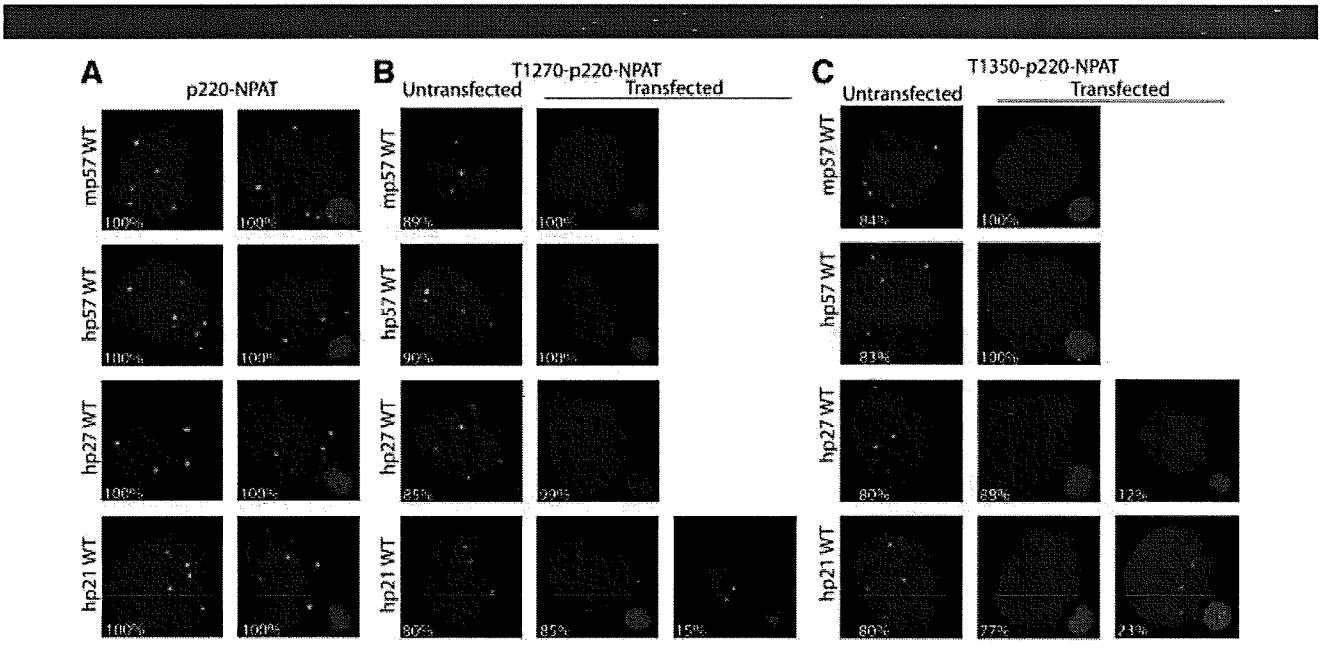

Fig. 3. $p57^{KIP2}$ selectively regulates the phosphorylation of $p220^{NPAT}$ at Cajal bodies. A–C: Immunofluorescence microscopy was performed on Cos7 cells with antibodies detecting endogenous $p220^{NPAT}$ (A), or CDK2 dependent phosphorylation at two distinct epitopes (i.e., T1270 (B) or T1350 (C)) in cells transfected with wild type human $p57^{KIP2}$, $p27^{KIP1}$, or $p21^{CIP1/WAF1}$ (right columns) or untransfected cells (left columns). Immunofluorescence signals (green) for total $p220^{NPAT}$, or the T1270 and T1350 phospho-epitopes are merged with DAPI signals (blue). The insets show merged image of cells transfected with wild type $p57^{KIP2}$, p27KIP1 or $p21^{CIP1/WAF1}$ (red; combined with DAPI to yield purple). The percentages on each part indicate the number of positive or negative cells.

Results

Irradiation reduces *histone* mRNA levels but not *histone* gene promoter activation by the p220^{NPAT}/HiNF-P complex

The CDK2 mediated phosphorylation of p220^{NPAT} as the co-activator of HiNF-P ensures the transcriptional activation of histone genes in conjunction with the onset of S phase. Therefore, it is necessary to understand how the activity of this transcriptional complex responds to inhibition of CDK activity that prevents cells from replicating DNA. *Histone* mRNA levels are rapidly degraded following inhibition of DNA synthesis (Baumbach et al., 1987; Stein et al., 1992). Indeed, we observe a rapid decrease of histone gene expression (e.g., *histone H4/n*) upon γ-irradiation of U2OS cells at a non-lethal dose (5 Gy), while *CDK2* and *GAPDH* mRNA levels are not affected (Fig. 1). Similar results for all parameters were obtained with a 12 Gy dose (data not shown). γ-Irradiation evokes a DNA damage response as reflected by an increase in *p21$^{CIP1/WAF1}$* mRNA levels at both 4 and 16 h after irradiation, while the mRNA levels of *p27^{KIP1}* decrease modestly and those of *p57^{KIP2}* remain relatively constant (Fig. 1).

Transfection assays with *histone H4* promoter/Luciferase reporter gene constructs show that γ-irradiation at 5 Gy does not affect activation of the *histone H4* gene promoter by HiNF-P and p220^{NPAT}, although p21$^{CIP1/WAF1}$ protein levels are clearly upregulated at both the 4 and 16 h time points (Fig. 2). Similar results were obtained upon increasing the radiation dose to 12 Gy (data not shown). Hence, physiological induction of p21$^{CIP1/WAF1}$ during a genotoxic stress response contributes to a reduction of *histone* mRNA accumulation but does not impinge on the CDK2 dependent transcriptional activation of *histone* genes by the p220^{NPAT}/HiNF-P complex. Our findings are in keeping with the longstanding observation that histone mRNA accumulation is dictated by both transcriptional and post-transcriptional mechanisms and that mRNA destabilization will override transcriptional activation (Baumbach et al., 1987; Stein et al., 1992).

Selective inhibition of p220^{NPAT} phosphorylation by CKIs at subnuclear foci

The finding that elevation of *p21$^{CIP1/WAF1}$* gene expression during a DNA damage response is not potent enough to block the activity of the p220^{NPAT}/HiNF-P transcriptional complex is unexpected. The data indicate that p220^{NPAT} phosphorylation may occur despite a reduction in cellular CDK kinase activity upon elevation of p21$^{CIP1/WAF1}$ levels. Therefore, we compared the potency of p21$^{CIP1/WAF1}$ in relation to the other two CKIs in regulating the in situ phosphorylation of p220^{NPAT} by CDK2 at subnuclear foci.

Phosphorylation of p220^{NPAT} by cyclin E/CDK2 at the G1/S boundary occurs on at least two distinct phospho-epitopes (T1270 and T1350) and is essential for activation of histone genes by HiNF-P (Ma et al., 2000; Mitra et al., 2003). Actively proliferating Cos7 cells typically have three to six p220^{NPAT} foci (Fig. 3A). Phosphorylation of p220^{NPAT} at both phospho-epitopes is observed in ~80–90% of the cells and predominantly in cells with more than three foci (Fig. 3B,C and data not shown). These data are consistent with the cell cycle specific phosphorylation of p220^{NPAT} during late G1 that persists throughout S and G2, as well as the expected doubling of p220^{NPAT} foci during S phase that has been observed in other cell types (Ma et al., 2000).

The focal organization of p220^{NPAT} is sustained upon introduction of exogenous p57^{KIP2}, p27^{KIP1}, or p21$^{CIP1/WAF1}$ (Fig. 3A). Forced expression of CKIs in each case reduces phosphorylation at both CDK2 related epitopes in transfected cells, but not in adjacent untransfected cells (Fig. 3B,C).

Importantly, p57^{KIP2} and p27^{KIP1} appear to be more effective than p21$^{CIP1/WAF1}$ in blocking p220^{NPAT} phosphorylation at T1270. We observe that none of the cells transfected with p57^{KIP2} and almost none of the p27^{KIP1} expressing cells (1% positive, 99% negative cells) are positive for phospho-T1270, while p21$^{CIP1/WAF1}$ expressing cells show residual immunoreactivity with the phospho-T1270 antibody (15% positive, 85% negative cells) (Fig. 3B). Moreover, p57^{KIP2} completely abrogates phosphorylation at T1350, while p27^{KIP1} (12% positive cells) and p21$^{CIP1/WAF1}$ (23% positive cells) do not (Fig. 3C). Our data suggest that p57^{KIP2} is more effective in blocking p220^{NPAT} phosphorylation in situ than the other two CKIs.

We tested the specificity of p57^{KIP2} to block p220^{NPAT} phosphorylation at subnuclear foci using p57^{KIP2} mutants (Fig. 4A). Both human and mouse wild type proteins are equally effective in blocking p220^{NPAT} phosphorylation (Fig. 4A,B). The CC and CCT mutants of p57^{KIP2} (see diagram in Fig. 6C below) are defective in cyclin binding and do not affect phosphorylation of p220^{NPAT} at T1270 or T1350 (Fig. 4A). Mutant p57^{KIP2}-T that lacks a CDK phosphorylation site required for Skp2 dependent degradation (Hattori et al., 2000) is equally effective as wild type

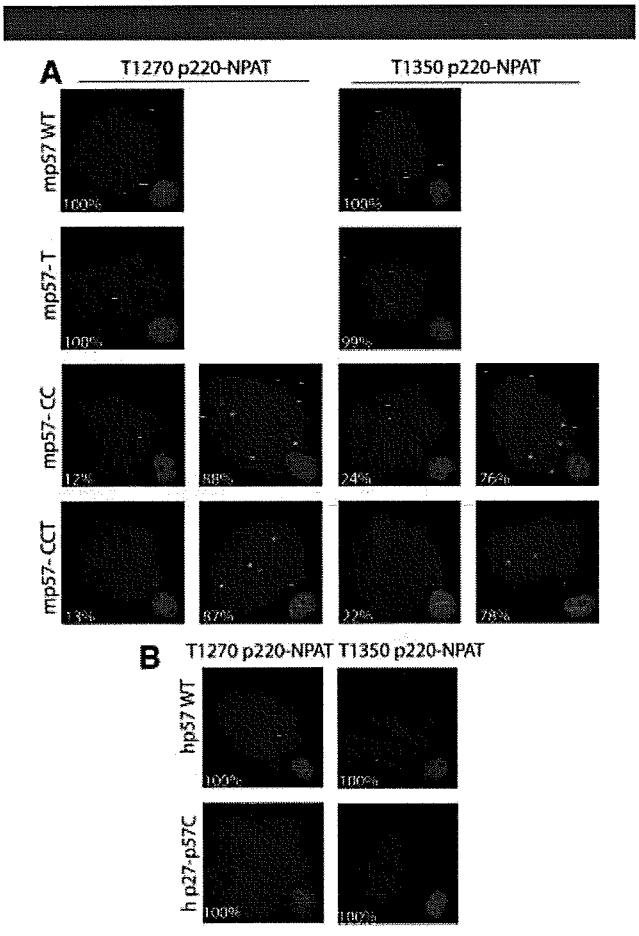

Fig. 4. Mutant p57^{KIP2} is defective in regulating in situ phosphorylation of p220^{NPAT}. A–B: Immunofluorescence microscopy detecting the T1270 or T1350 epitopes (green) was performed as described in Figure 1 using cells transfected with wild type mouse p57^{KIP2} or three different mutants (i.e., p57^{KIP2}-T, -CC, or -CCT) (A) or human p57^{KIP2} compared with a human p27^{KIP1}–p57^{KIP2} chimera (B). Insets show merged images of p57^{KIP2} (red) and DAPI signals (blue) in transfected cells. The percentages on each part indicate the number of cells with a microscopic phenotype.

(Fig. 4). Thus, in situ inhibition of $p220^{NPAT}$ apparently requires the functional cyclin binding domain of $p57^{KIP2}$.

The structure of $p57^{KIP2}$ differs from $p27^{KIP1}$ by the presence of a C-terminal proline-alanine extension (PAPA repeat) (Matsuoka et al., 1995) that is similar but not entirely identical in mouse and human. Despite only partial conservation of the C-terminus, both human and mouse $p57^{KIP2}$ are similarly effective in blocking $p220^{NPAT}$ phosphorylation (Fig. 4A,B). To examine the contribution of the C-terminus, we prepared a chimera in which the C-terminus of human $p57^{KIP2}$ is fused to the N-terminal cyclin binding domain of $p27^{KIP1}$. The $p27^{KIP1}$–$p57^{KIP2}$ chimera is as effective as wild type $p57^{KIP2}$ in blocking T1270 and T1350 phosphorylation of $p220^{NPAT}$ (Fig. 4B). Hence, our data suggest that the selective ability of human $p57^{KIP2}$ to prevent $p220^{NPAT}$ phosphorylation is mediated in part by its unique C-terminus.

$p57^{KIP2}$ is the most effective inhibitor of the cyclin E/CDK2/$p220^{NPAT}$/HiNF-P pathway

Phosphorylation of $p220^{NPAT}$ is inhibited by the three CKIs in part due to reduced CDK2 kinase activity as measured using histone H1 as a substrate (Fig. 5A). Under our experimental conditions, $p27^{KIP1}$ is a stronger inhibitor of CDK2 activity than $p57^{KIP2}$ or $p21^{CIP1/WAF1}$ (Fig. 5A). Hence, the relative intrinsic strength by which CKIs inhibit CDK2 kinase activity does not appear to correlate directly with their ability to reduce phosphorylation of the two epitopes of $p220^{NPAT}$.

We tested the functional effects of the three CKIs on HiNF-P/$p220^{NPAT}$ co-activation using *histone H4* gene reporter assays (Fig. 5B). Forced expression using limited amounts of expression vector elevates the levels of $p57^{KIP2}$, $p27^{KIP1}$, and $p21^{CIP1/WAF1}$ (Fig. 5B), but only $p57^{KIP2}$ elevation represses the HiNF-P/$p220^{NPAT}$ dependent stimulation of *H4* gene transcription at the doses shown here (Fig. 5B). We note that $p21^{CIP1/WAF1}$, $p27^{KIP1}$, and $p57^{KIP2}$ can each block *histone H4* gene promoter activity in a dose-dependent manner when exogenously expressed at higher levels, although $p57^{KIP2}$ still remains more effective than $p27^{KIP1}$ or $p21^{CIP1/WAF1}$ (data not shown). Excessive non-physiological levels of CKIs will result in a general block of CDK2 activity thus indiscriminately suppressing the phosphorylation of $p220^{NPAT}$ and preventing activation of transcription by the $p220^{NPAT}$/HiNF-P complex. We also examined the effect of the F-box protein Skp2, which promotes $p57^{KIP2}$ degradation (Kamura et al., 2003), on activation of the *H4* gene promoter. Co-expression of Skp2 decreases $p57^{KIP2}$ and restores the ability of $p220^{NPAT}$ and

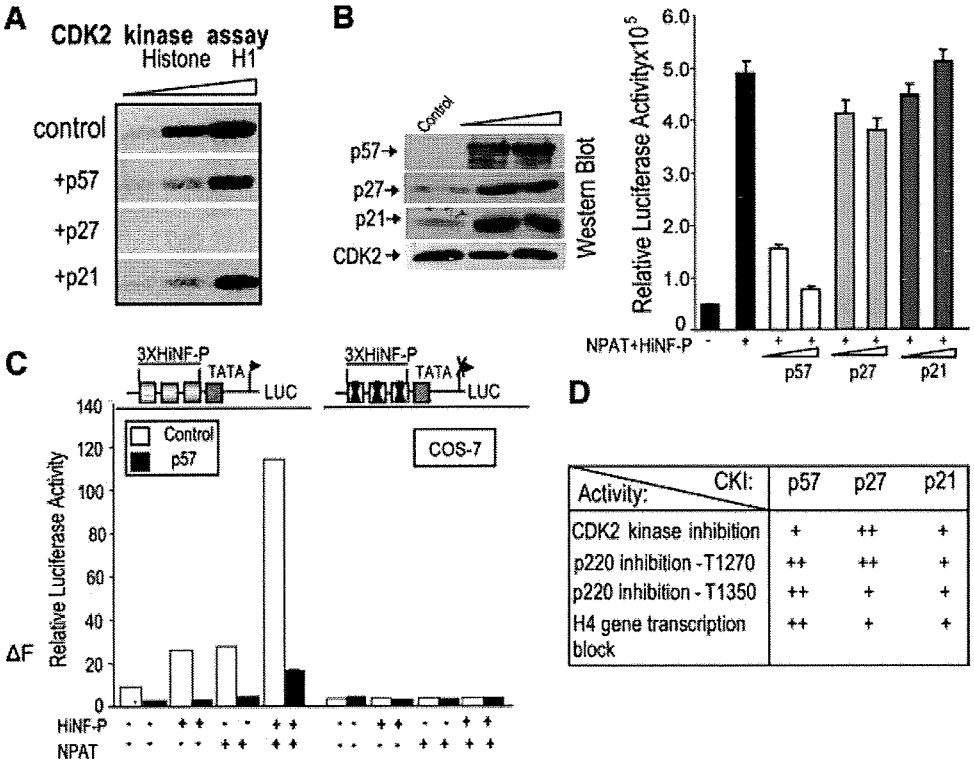

Fig. 5. Inhibition of CDK2 kinase activity and *H4* gene transcription by $p57^{KIP2}$. A: In Cos7 lysates, $p27^{KIP1}$ is more potent than $p57^{KIP2}$ or $p21^{WAF1/CIP1}$ in blocking CDK2 activity. CDK2 kinase activity was measured using γ-^{32}P-ATP and histone H1 as a substrate in CDK2 immunoprecipitates (respectively, 2, 5, and 10 μl of beads) obtained with lysates of mock-transfected cells or cells expressing $p57^{KIP2}$, $p27^{KIP1}$, or $p21^{WAF1/CIP1}$. B: Selective inhibition of HiNF-P/$p220^{NPAT}$ signaling at the *H4* promoter by $p57^{KIP2}$. Co-transfection experiments with a wild type *H4* promoter-luciferase reporter gene in the absence (first bar) or presence of vectors for HiNF-P (200 ng/well) or $p220^{NPAT}$ (150 ng/well) (remaining bars) in cells expressing exogenous CKIs (25 or 50 ng vector) as indicated. *H4* promoter-luciferase activities were measured within 24 h after transfection and plotted as a function of $p57^{KIP2}$ vector concentration (right part). Western blot analysis (left part) was used to examine CKI expression in whole cell lysates (20 μg protein). Note that Cos7 cells do not express endogenous $p57^{KIP2}$. C: The HiNF-P binding site is sufficient for $p57^{KIP2}$ dependent inhibition of the *H4* gene promoter. Cos7 cells were co-transfected with Luciferase reporters controlled by wild type or mutant HiNF-P elements fused to a minimal TATA box promoter. Relative promoter activity was assessed in the presence (+) or absence (–) of vectors expressing HiNF-P, $p220^{NPAT}$, or $p57^{KIP2}$ (25 ng/ml) as above. D: Summary of data presented in Figures 1–3 with + signs indicating the relative effectiveness of CKIs to affect the activities in the left column.